NUMERICAL AND EXPERIMENTAL INVESTIGATIONS FOR IMPROVING DIELECTRIC MEASUREMENTS WITH MICROWAVE CAVITIES

A Thesis Submitted to
the Graduate School of
İzmir Institute of Technology
in Partial Fulfillment of the Requirements for the Degree of

MASTER OF SCIENCE

in Electronics and Communication Engineering

by
Ceren ÖZKAL

July 2020
İZMİR

ACKNOWLEDGMENTS

I would first like to express my sincere appreciation to my supervisor Assist. Prof. Dr. Fatih YAMAN for his impressive guidance, encouraging me to research and tolerance he showed at every stage of my thesis. He allowed this study to be my own work but led me in the right direction whenever he thought I needed it. I would also like to thank the thesis defense committee members, Prof. Dr. Valery G. YAKHNO and Assoc. Prof. Dr. Kıvılcım YÜKSEL ALDOĞAN for their valuable suggestions and constructive comments on this thesis. I am also grateful to Dr. Ing. Fritz CASPERS for its recommendation to increase the accuracy of power measurement inside the cavity.

I express my profound gratitude to my mother Nesibe ATİLA for her unfailing support and continuous encouragement. This accomplishment would not have been possible without her. I am also grateful to dear Anıl KARATAY for his persistent help and valuable support. Special thanks to Hasan Önder YILMAZ, Ertunga Burak KOÇAL and Oğulcan ERDOĞAN.

Finally, I would like to thank my institution for the financial support it provides me.

ABSTRACT

NUMERICAL AND EXPERIMENTAL INVESTIGATIONS FOR IMPROVING DIELECTRIC MEASUREMENTS WITH MICROWAVE CAVITIES

In this thesis, by utilising the inverse scattering problems approach, it was tried to improve the sensitivity in measuring the dielectric constants of the materials with microwave resonator cavities. The direct problem involves measurement of frequency shift and electric field/power values. The inverse problem aims to calculate the dielectric constant with the data obtained from the direct problem. First of all, the accuracy of the rectangular and cylindrical cavities operating in the S-band in the material perturbation method was compared with simulations, and how their sensitivity changes depending on the increasing frequency and dielectric constant was observed. Afterwards, dielectric constants were calculated by measuring the frequency shifts in the scope of the direct problem with a rectangular aluminium cavity for 3 different materials at the frequency of 1.254 GHz. However, this traditional method has a high error rate especially for samples with large dielectric constant or volume. For this reason, a measurement method based on Newton-Raphson iteration approach has been proposed. This proposed method uses power or electric field measurements at a particular frequency regardless of which mode is excited in the cavity. With the help of iterations based on an initial guess, the dielectric constant could be determined more precisely. Within the scope of this thesis, the results of the simulations performed with the Newton-Raphson method were given and the effect of the change of 3 different parameters of the method on the results was observed. In these simulations, iterations were carried out using electric field values at a certain number of points around the material. Finally, with the help of the spectrum analyzer, power mea-surements were taken from the 7-port aluminium cavity for the direct problem and the inverse scattering problem, which aims to recalculate the dielectric constant, was solved. More accurate results were obtained with the Newton-Raphson method.

ÖZET

MİKRODALGA KAVİTELER İLE DİELEKTRİK ÖLÇÜMLERİNİN GELİŞTİRİLMESİ İÇİN NÜMERİK VE DENEYSEL ARAŞTIRMALAR

Bu tezde, ters saçılma problemleri yaklaşımından faydalanarak mikrodalga rezonatör kavitelerle materyallerin dielektrik katsayılarının ölçümünde hassasiyet iyileştirilmeye çalışılmıştır. Düz problem frekanstaki kayma ve elektrik alan/güç değerlerinin ölçülmesini kapsar. Ters problem ise düz problemden elde edilen verilerle dielektrik sabitini hesaplamayı amaçlar. Öncelikle, simülasyon ortamında S bandında çalışan dikdörtgen ve silindirik kavitelerin materyal pertürbasyon yöntemindeki doğrulukları kıyaslanmış, artan frekans ve dielektrik sabitine bağlı olarak hassasiyetlerinin ne yönde değiştiği gözlemlenmiştir. Ardından, dikdörtgen bir alüminyum kavite ile 1.254 GHz frekansında 3 farklı malzeme için aynı yöntemle düz problem kapsamında frekanstaki kaymalar ölçülerek dielektrik sabitleri hesaplanmıştır. Ancak özellikle dielektrik sabiti veya hacmi büyük olan maddeler için bu geleneksel yöntem yüksek hata oranına sahiptir. Bu nedenle Newton-Raphson iterasyon yaklaşımına dayanan bir ölçüm yöntemi önerilmiştir. Önerilen bu yöntemde, kavite içinde hangi modun uyarıldığına bakmaksızın belirli bir frekanstaki güç veya elektrik alan ölçümlerinden faydalanılmaktadır. Bir başlangıç tahmininden yola çıkarak yapılan iterasyonlar yardımıyla dielektrik sabiti daha hassas bir şekilde belirlenebilmiştir. Bu tez kapsamında, Newton-Raphson yöntemi ile yapılan simülasyonların sonuçları paylaşılmış ve yönteme ait 3 farklı parametrenin değişiminin sonuçlar üzerindeki etkisi gözlemlenmiştir. Bu simülasyonlarda materyalin çevresindeki belirli sayıda noktadaki elektrik alan değerleri kullanılarak iterasyonlar gerçekleştirilmiştir. Son olarak, spektrum analizör yardımıyla 7 portlu alüminyum kaviteden düz problem için güç ölçümleri alınmış ve dielektrik sabitini yeniden hesaplamayı amaçlayan ters saçılma problemi çözülmüştür. Newton-Raphson yöntemiyle daha doğru sonuçlar elde edilmiştir.

TABLE OF CONTENTS

LIST OF FIGURES

Figure **Page**

Figure **Page**

LIST OF TABLES

LIST OF ABBREVIATIONS

EM . . . . . Electromagnetic
TE . . . . . Transverse Electric
TM . . . . . Transverse Magnetic
FEM . . . . . Finite Element Method
FIT . . . . . Finite Integration Technique
CST . . . . . Computer Simulation Technology
MWS . . . . . Microwave Studio
VNA . . . . . Vector Network Analyzer
SA . . . . . Spectrum Analyzer
dB . . . . . Decibel
dBm . . . . . Decibel-milliwatts

CHAPTER 1

INTRODUCTION

The electrical properties of each material are different depending on their dielectric characteristics. Determination of dielectric characteristics is related to dipolar and atomic polarizations. The earliest investigations on polarizability and dielectric materials belong to Debye (1929). Von Hippel has analyzed the dielectrics more comprehensively (1954b) and has studied on dielectric measurements and applications (1954a).

Since the dielectric constant was related to the temperature and the amount of water contained in the fruits and vegetables, dielectric measurements of foodstuffs have been performed for storage and feasibility information (Dunlap and Makower, 1945). Measurements became the most valuable agricultural practice when first used to determine the moisture content of grains (Nelson, 1965). Through the development of microwave heating applications, the efficiency of dielectric measurements was noticed in determining and improving the heating time and amount of heat. Today, researches in the food industry are still carried out (Clerjon and Damez, 2009).

Dielectric measurements take place in a wide variety of areas, such as calculating the water hardness in cooling systems (Teng et al., 2017) or designing high-frequency electronic circuits (Riedell et al., 1990). To develop radiation-absorbing materials in the defence industry, the dielectric characterizations of materials must be known. Another example is radars that can detect objects behind obstacles. The dielectric property information of the obstacle is used to increase accuracy, as reflected and lost signals will be affected. So we can say that understanding the response of materials to electromagnetic (EM) fields is significant for many research and development projects.

1.1. Permittivity Measurement Techniques

As technology improves, the variety of permittivity measurement methods has increased over the years. Baker-Jarvis et al. (2010) prepared a classification system to choose an appropriate measurement method according to sample preparation, measurement accuracy, frequency band, sample characterization etc. In the microwave frequency range, we can examine these measurement techniques under two main titles as

non-resonant and resonant methods (Jilani, 2012).

1.1.1. Non-Resonant Methods

Non-resonant methods can also be called transmission-reflection methods. The electromagnetic wave is transmitted over the material and the power of the wave reflected from the material is measured. It is sufficient to find the reflection coefficient (S_{11}) and the transmission coefficient (S_{21}) to determine the complex permittivity. Non-resonant methods can be performed in closed conditions such as coaxial and waveguides, or in free-space with one or two antennas. (Krupka, 2006)

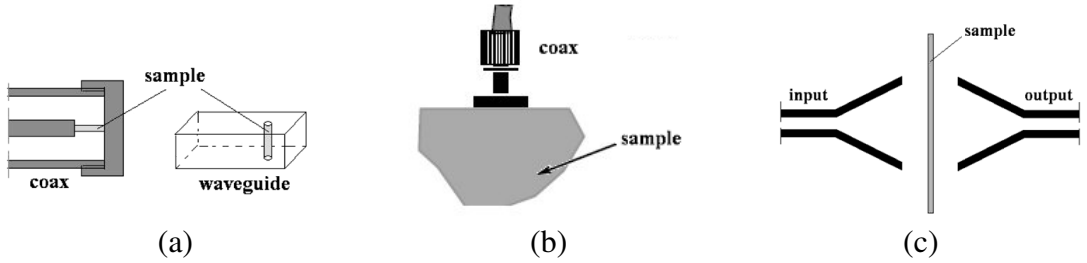

(a) (b) (c)

Figure 1.1. Non-resonant measurement methods (a) Transmission line method (Source: Krupka, 2006) (b) Open-ended probe method (Source: Jilani, 2012) (c) Free space method (Source: Krupka, 2006)

Coaxial cables and waveguides are used in the transmission line method as shown in Figure 1.1.a. The material of unknown permittivity is placed into the transmission line and the rate of change in power is calculated. Liquids give more precise results than solids due to their air-gap structures. This method generally works in broadband but the waveguide gives more sensitive results compared to the coaxial line while remaining in the narrower band (Ogunlade et al., 2006 ; Jiqing Hu et al., 2006).

In Figure 1.1.b, the open-ended probe method is shown. This non-destructive method is utilised especially on foods (Nelson and Bartley, 2002) and biological tissues (R. Zajicek, 2006). By measuring only the reflection coefficient (S_{11}), the complex permittivity is achieved. Although it is the fastest and easiest method, it is one of the least sensitive and difficult to calibrate methods.

In the free space method, two antennas can be used as shown in Figure 1.1.c, or a single antenna can be used. It is an uncomplicated and quick method that can be selected

when it is not desired to damage the material (Wee et al., 2009). The most critical problem to consider is the necessity to use a focused beam to avoid diffraction at the edges of the sample. The distance between the antennas and the distance of the sample to the antennas should be calculated correctly. As in transmission line methods, permittivity is calculated with reflection and transmission coefficients (Ghodgaonkar et al., 1990).

1.1.2. Resonant Methods

In the resonant methods, as shown in Figure 1.2, open resonators and different cavities such as rectangular (Jha and Akhtar, 2014), cylindrical (Shihe Li et al., 1981), re-entrant cavities (Kaczkowski and Milewski, 1980) can be used as well as the material itself can form a dielectric resonator (Hakki and Coleman, 1960; Shu and Wong, 1995). The least error rate in permittivity measurements is in the resonant methods.

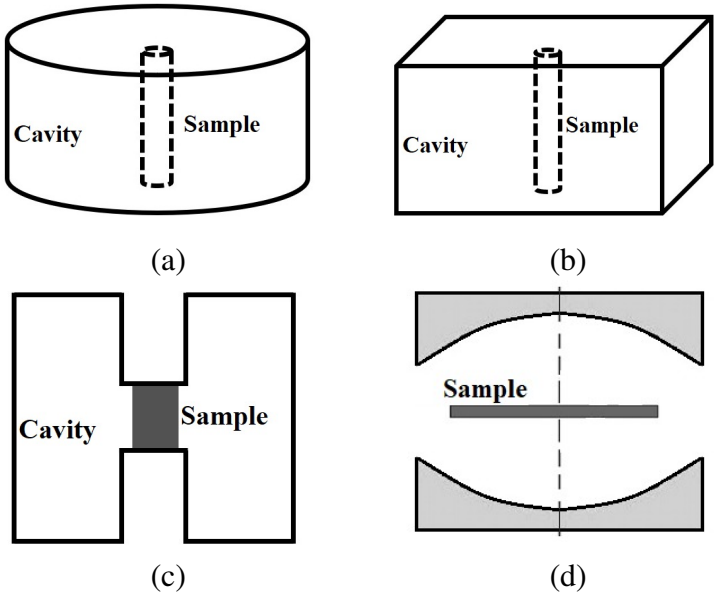

Figure 1.2. Resonant measurement methods (a) Cylindrical cavity (b) Rectangular cavity (c) Re-entrant cavity (d) Open resonator

As shown in Figure 1.2, closed cavity structures can be formed in different shapes. The aim at closed cavity structures is to confine electromagnetic energy. Thus, electromagnetic patterns called mode occur inside the cavity. In the open resonator method, as in the free space method, the material must be sufficiently big so that the diffraction at

the edges of the material does not cause the radiation loss. Dielectric measurement with cavities is based on the perturbation theory. The reference values are obtained when the cavity is empty and then, the measured values after the sample is placed are used to find the permittivity. The energy stored in the resonator cavity is greater than the energy on the sample, whereas, in dielectric resonators, almost total of the energy is stored on the material. In the dielectric resonator method, the sample is placed between two conductive metal shields or inside the metal cavity to reduce the radiation loss as much as possible. The measurement of complex permittivity in the dielectric resonators gives more accurate results than the cavity perturbation method (Sheen, 2007).

1.2. Motivation

Resonator cavity method in the dielectric measurements is widely used since it gives high accuracy results. However, the perturbation technique has limitations on the operating frequency and the size and shape of the material under test(Ozkal and Yaman, 2019). The amount of sample volume in the perturbation approach is effective on the error rate of the reconstructed dielectric constant (Ozkal and Yaman, 2018). The ratio of the maximum material volume to the cavity volume with limited frequency shift and the effect of the material geometry (rod, disk and sphere) on the measurement results have been tested for the most precise results (Peng et al., 2014). Investigations have been carried out on different cavity structures such as a cavity formed with a double ridged waveguide to enhance the operating frequency (Kik, 2016). There are also examinations where a filling hole has been added to the cover of the cavity to make applicability more practical (Kilic et al., 2013; Nishikata, 2009). In these studies, it was observed that the effect of the hole cannot be neglected and this effect was calculated for the cavity structures in the examinations. The assumptions of the perturbation theory are not always adequate for dielectric measurements in the development of the resonator methods (Carter, 2001a).

Santra and Limaye (2005) used the Newton-Raphson iteration method instead of the perturbation approach in measuring the dielectric constant with resonator cavities. The iteration method has been confirmed to be successful in materials with arbitrary shape and high loss in determining the dielectric constant. This proposed approach removed the dependence on the volume of the material while providing reliable results in materials with high dielectric constant. This method is very beneficial as it can operate on all frequency bands. In their study, 3 different modes were excited and therefore took measurements for 3 different frequencies.

In this thesis, it is mentioned that the dielectric constant of a material can be detected in the cavity without the need for a particular mode excitation. By choosing a frequency without considering a certain mode, the Newton-Raphson iteration technique is implemented by analysing the electric field or power distribution in the cavity with the contribution of neighbouring modes of that frequency. Measured values obtained from a material whose dielectric constant is known are used as the initial point. From the difference between the initial point and the measurement results obtained with the sample whose dielectric constant is unknown, the result is approached by the iteration method. Thus, no matter how high the dielectric constant is, the parameter indicating the electrical property of the material can be determined. The absence of dependence on resonance frequency and sample volume in this technique provides a prominent advantage in the application of the approach.

CHAPTER 2

THEORETICAL BACKGROUND

This section is devoted to some necessary information about the dielectric constant and the complex permittivity. The section will continue by giving mathematical background information of the material perturbation method and the proposed Newton-type approach, and by explaining the applications of the methods to dielectric measurements.

2.1. Permittivity and Dielectric Constant

When specifying on the scopes where electromagnetic materials are used in microwave frequencies, the responses of the materials to electromagnetic fields are considered. Non-metallic materials with high insulation resistance to the electric field and used to store electrical charges are classified as dielectrics. Fundamentally non-metallic materials that provide electrical insulation are called insulators. Non-metal materials whose function is to store electrical charges are dielectric. When dielectrics are exposed to an electric field, instead of current flowing through them like metals, electric polarization that reduces the electric field occurs. (Chen et al., 2004)

Permittivity ϵ determines the dielectric characterization of the material and is a complex expression. The relationship between the real and imaginary parts of the complex permittivity gives us information about its resistance to electricity. If the real part of the permittivity ϵ' is larger, it can be said that the material is included in the dielectric type, while the imaginary part ϵ'' is higher, it can be said that the material is metal.

$$\epsilon_r = \frac{\epsilon}{\epsilon_0} = \frac{\epsilon' - j\epsilon''}{\epsilon_0} = \epsilon'_r - j\epsilon''_r \tag{2.1}$$

The dielectric constant ϵ_r is the ratio of the complex permittivity to the free-space permittivity ϵ_0 as seen in Equation (2.1) and is also called the relative complex permittivity due to be frequency-dependent for time-varying electromagnetic fields. While the unit of the complex permittivity is Farad/meter, the dielectric constant is unitless.

When the dielectric sample is exposed to an electric field, four types of polarization occur. These are electronic, ionic, orientational and space charge polarizations. All polarizations occur at low frequencies so that total polarization is high. But as the frequency increases, total polarization decreases. Thus, the dielectric constant becomes frequency-dependent. Within the scope of this thesis, chose samples under test have the same dielectric constant value at the operating frequency range.

Besides the frequency, the temperature also affects the dielectric constant. Orientational and space charge polarizations are affected by temperature, so the dielectric constant of material also changes with temperature. In this thesis, experiments were carried out at room temperature.

2.2. Material Perturbation Theory

The cavity perturbation method utilised the material perturbation theory and is an approximate technique for the measurement of electromagnetic properties of a material in microwave frequencies. When a small amount of dielectric or magnetic material that has arbitrary shape is inserted into a microwave resonator cavity, the electric and magnetic fields are perturbed, and this causes a shift in the resonant frequency and a change of the quality factor (Pozar, 2012 ; Carter, 2001b).

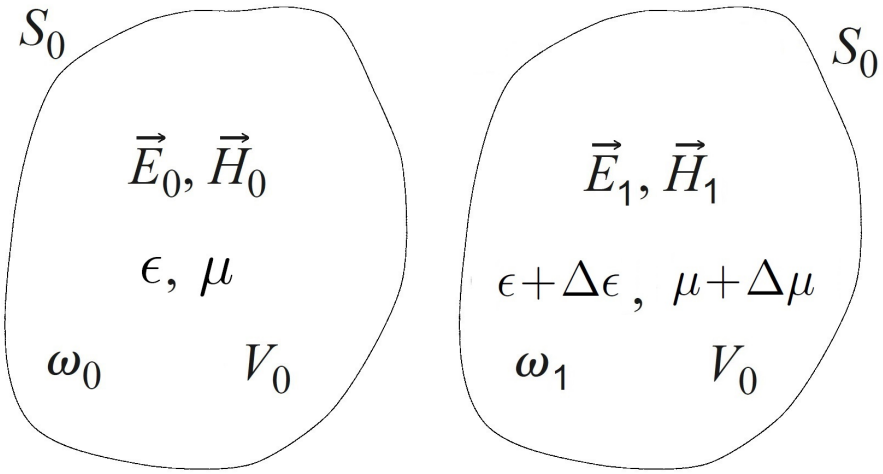

Figure 2.1. Material perturbation of an arbitrarily shaped cavity

Material perturbation in a resonator cavity is based on the difference in the permittivity ($\Delta\epsilon$) or the permeability ($\Delta\mu$) of an introduced material as shown in Figure 2.1. $\vec{E}_0$ and $\vec{H}_0$ represent the electric and magnetic fields of the unperturbed cavity and they become $\vec{E}_1$ and $\vec{H}_1$ after the small-sample perturbation. According to Maxwell's equations, fields can be expressed as

$$\nabla \times \vec{E}_0 = -j\omega_0\mu\vec{H}_0 \tag{2.2}$$

$$\nabla \times \vec{H}_0 = j\omega_0\epsilon\vec{E}_0 \tag{2.3}$$

$$\nabla \times \vec{E}_1 = -j\omega_1(\mu + \Delta\mu)\vec{H}_1 \tag{2.4}$$

$$\nabla \times \vec{H}_1 = j\omega_1(\epsilon + \Delta\epsilon)\vec{E}_1 \tag{2.5}$$

where ω_0 is the angular resonant frequency of the unperturbed cavity and ω_1 shows the angular resonant frequency of the perturbed cavity. If a lossy material is used, then the change in frequency will be a complex value. When the complex conjugate of Equation (2.2) is multiplied by $\vec{H}_1$ and Equation (2.5) is multiplied by $\vec{E}_0^*$, Equations (2.6) and (2.7) are obtained.

$$\vec{H}_1 \cdot \nabla \times \vec{E}_0^* = j\omega_0\mu\vec{H}_1 \cdot \vec{H}_0^* \tag{2.6}$$

$$\vec{E}_0^* \cdot \nabla \times \vec{H}_1 = j\omega_1(\epsilon + \Delta\epsilon)\vec{E}_0^* \cdot \vec{E}_1 \tag{2.7}$$

Using the vector identity in Equation (2.8), when the Equations (2.6) and (2.7) are subtracted from each other, the Equation (2.9) is achieved.

$$\nabla \cdot (\vec{A} \times \vec{B}) = \vec{B} \cdot \nabla \times \vec{A} - \vec{A} \cdot \nabla \times \vec{B} \tag{2.8}$$

$$\nabla \cdot (\vec{E}_0^* \times \vec{H}_1) = j\omega_0 \mu \vec{H}_1 \cdot \vec{H}_0^* - j\omega_1(\epsilon + \Delta\epsilon)\vec{E}_0^* \cdot \vec{E}_1 \tag{2.9}$$

By repeating similar operations, the complex conjugate of Equation (2.3) is multiplied by $\vec{E}_1$ and Equation (2.4) is multiplied by $\vec{H}_0^*$. Subtracting Equations (2.10) and (2.11) by using the vector identity in Equation (2.8) gives Equation (2.12).

$$\vec{E}_1 \cdot \nabla \times \vec{H}_0^* = -j\omega_0 \epsilon \vec{E}_1 \cdot \vec{E}_0^* \tag{2.10}$$

$$\vec{H}_0^* \cdot \nabla \times \vec{E}_1 = -j\omega_1(\mu + \Delta\mu)\vec{H}_0^* \cdot \vec{H}_1 \tag{2.11}$$

$$\nabla \cdot (\vec{E}_1 \times \vec{H}_0^*) = -j\omega_1(\mu + \Delta\mu)\vec{H}_0^* \cdot \vec{H}_1 + j\omega_0 \epsilon \vec{E}_1 \cdot \vec{E}_0^* \tag{2.12}$$

Equations (2.9) and (2.12) are added and integrated over the volume of the cavity V_0. Gauss' theorem provides that the integral over the volume transform to the integral over the enclosed surface. When the cavity material is perfectly conducting, the electric field is normal and the magnetic field is tangential to the surface. Thus, the Equation (2.13) becomes equal to zero. The integral expression can be rewritten as in Equation (2.14).

$$\int_{V_0} \nabla \cdot (\vec{E}_0^* \times \vec{H}_1 + \vec{E}_1 \times \vec{H}_0^*) \mathrm{d}v = \oint_{S_0} (\vec{E}_0^* \times \vec{H}_1 + \vec{E}_1 \times \vec{H}_0^*) \cdot \mathrm{d}\vec{s} = 0 \tag{2.13}$$

$$j \int_{V_0} \Big((\omega_0 \epsilon - \omega_1[\epsilon + \Delta\epsilon])\vec{E}_0^* \cdot \vec{E}_1 + (\omega_0 \mu - \omega_1[\mu + \Delta\mu]\vec{H}_0^* \cdot \vec{H}_1) \Big) \mathrm{d}v = 0 \tag{2.14}$$

If the cavity is perfect conductive, Equation (2.15) is the fundamental equation for the deduction of the electromagnetic properties of the sample by material perturbation.

$$\frac{\omega_0 - \omega_1}{\omega_1} = \frac{\int_{V_0}(\Delta\epsilon\vec{E}_1 \cdot \vec{E}_0^* + \Delta\mu\vec{H}_1 \cdot \vec{H}_0^*)\mathrm{d}v}{\int_{V_0}(\epsilon\vec{E}_1 \cdot \vec{E}_0^* + \mu\vec{H}_1 \cdot \vec{H}_0^*)\mathrm{d}v} \tag{2.15}$$

The fundamental equation of the material perturbation is not calculable because of expressions of perturbed cavity fields. However, even if a sample with high permittivity or permeability is used, the total perturbation will be weak since the sample volume will be small. In this case, since the change in the system is small to not disturb the mode distribution, the unperturbed and perturbed field expressions are close to each other, and $\vec{E}_0$ and $\vec{H}_0$ can be written directly instead of $\vec{E}_1$ and $\vec{H}_1$ as in Equation (2.16).

$$\frac{\omega_0 - \omega_1}{\omega_0} \approx \frac{\int_{V_0}(\Delta\epsilon|\vec{E}_0|^2 + \Delta\mu|\vec{H}_0|^2)\mathrm{d}v}{\int_{V_0}(\epsilon|\vec{E}_0|^2 + \mu|\vec{H}_0|^2)\mathrm{d}v} \tag{2.16}$$

Equation (2.16) gives the information that an increase in permittivity or permeability will cause a decrease in resonant frequency. The angular resonant frequency is a complex value, $\omega = \omega_r + j\omega_i$. The resonant frequency is expressed as $f = \omega_r/2\pi$, and the quality factor is calculated from $Q = \omega_r/2\omega_i$. Since the quality factor is very high in perfectly conducting structures, the imaginary part can be ignored.

In permittivity measurements, the sample used is non-magnetic, so the permeability difference ($\Delta\mu$) goes to zero. The integral expression in the numerator of Equation (2.16) can be calculated over the sample volume since the permittivity does not change outside the sample. Equation (2.17) is reached with the assumption that the sample volume is too small where V_s represents the volume of the sample.

$$\frac{\omega_0 - \omega_1}{\omega_0} \approx \frac{\int_{V_s}\Delta\epsilon|\vec{E}_0|^2\mathrm{d}v}{2\int_{V_0}\epsilon|\vec{E}_0|^2\mathrm{d}v} \tag{2.17}$$

The sample is put in the centre where the electric field is maximum. Electric field expressions are calculated by substituting in Equation (2.17) for rectangular and

cylindrical cavities and a dielectric constant equation is obtained. The general expression of the dielectric constant equation is stated as

$$\frac{\Delta\epsilon}{\epsilon} = \xi \frac{V_c}{V_s} \frac{\omega_0 - \omega_1}{\omega_0} \tag{2.18}$$

where ξ is 0.5 for TE_{101} mode of a rectangular cavity and 0.539 for TM_{010} mode of a cylindrical cavity. V_c and V_s indicate the cavity and the sample volumes respectively. $\Delta\epsilon$ shows the dielectric constant difference between the empty cavity and the dielectric-loaded cavity.

2.3. Newton-Raphson Method

The Newton-Raphson method is a technique of finding the roots of a given function. The idea belongs to Newton, and Raphson writes the equation in the final form so the method is called by the two. In other root-finding methods such as secant and bisection, at least two points and their outputs are required, while in Newton method one point and its output, and the derivative value with the tangent line passing through that point are sufficient. It is one of the most used methods for optimization in science and engineering because it is simple and easily applicable (Ostrowski, 1966).

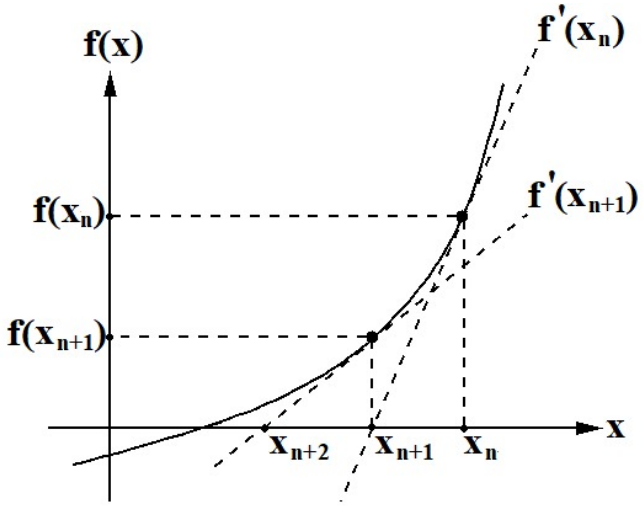

Figure 2.2. Geometrical representation of the Newton-Raphson method

The Newton method is based on solving the scalar equation $f(x) = 0$, where f is a continuous function. A tangent line is drawn using the known point (x_n, $f(x_n)$) on the graph of $f(x)$. After the derivative of $f(x_n)$, $f'(x_n)$ from the tangent line is achieved, the equation is written as Taylor polynomial as in Equation (2.19).

$$f(x_n) + (x_{n+1} - x_n)f'(x_n) = 0 \tag{2.19}$$

In Figure 2.2, $f'(x_n)$ can be written as $f'(x_n) = f(x_n)/(x_n - x_{n+1})$ since it means the slope of the tangent line. Thus, x_{n+1} is assigned at the intersection point between the tangent line and the x-axis and can be written as in Equation (2.20).

$$x_{n+1} = x_n - \frac{f(x_n)}{f'(x_n)} \tag{2.20}$$

The sequence of x_n values is obtained consequently, and this sequence becomes the linear interpolation of $f(x)$. x_n sequence produces an iterative solution and the point where the iteration converges, gives the root of $f(x)$.

When the Newton-Raphson method is applied to dielectric measurements, the electric field or power values of a material whose dielectric constant is known are determined at the first step. The known dielectric constant forms the initial guess. If the initial guess value is not close to the root of the function sufficiently, the Newton-Raphson technique may not converge or may converge to the false root. Then, the initial point is approached by iterations from the electric field or power measurements of the sample whose dielectric properties are indefinite. Thus, unknown dielectric constant information is obtained. The steps to be followed are described in the flow chart in Figure 2.3.

This part of the problem can be considered as a direct scattering problem for an object located inside of a bounded domain and the solution of the problem is finding the electric field/power on a certain line inside the domain. Accordingly, the inverse problem can be imagined as reaching the unknown dielectric parameter of the material from the data obtained in the direct problem. In this thesis, the direct problem is calculated with two approaches, by Finite Element Method which is implemented in the 3D electromagnetic field solver, i.e. CST-MWS and by measurements via Spectrum Analyser. For the solution of the inverse problem, we used a Newton iterative type algorithm.

Within the scope of this thesis, in order to find the dielectric constant of an unknown material we first excite the cavity at the frequency which does not correspond to any of its resonant frequencies. Afterwards, we achieve the magnitude of the electric fields or powers inside the cavity at certain points on a circle around the material.

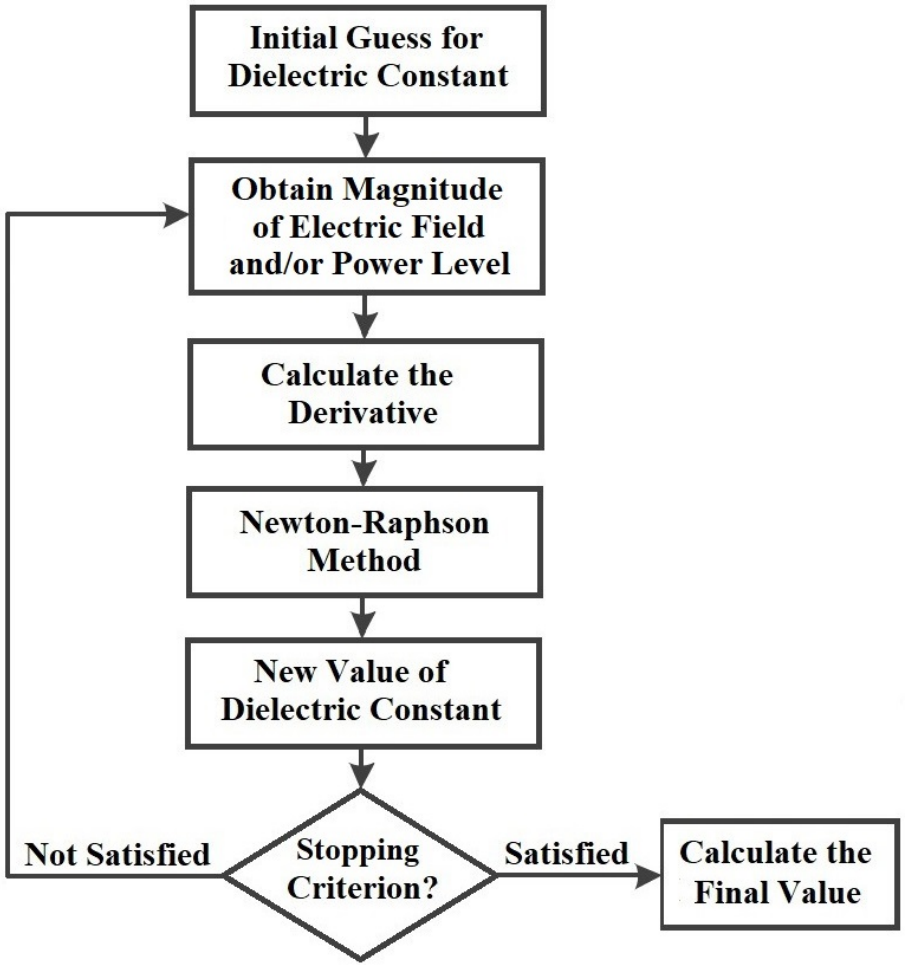

Figure 2.3. Flowchart of Newton-Raphson method in dielectric measurements

The main equation to be solved iteratively is given in Equation (2.21). ϵ_x denotes the dielectric constant of the sample whose electrical properties are unknown. $F(\epsilon_x)$ indicates the magnitude of the measured electric field or power expression when the dielectric constant is ϵ_x. ϵ_1 shows the known dielectric constant as the initial guess while $F(\epsilon_1)$ gives the magnitude of the measured electric field or power values. Measuring from more points makes the result more precise. The points to be measured are optimally adjusted according to the way the sample is placed in the cavity.

$$|F(\epsilon_x)| = |F(\epsilon_1)| + |F'(\epsilon_1)|h \tag{2.21}$$

$F'(\epsilon_1)$ represents the numerical derivative of $F(\epsilon_1)$ and can be calculated from Equation (2.22) with Δ value as the difference quotient. Δ value should be chosen so that the numerical derivative does not go to zero. Accordingly, in the numerical implementation, we check the related derivative if it is sufficiently large at each iteration step. h parameter is achieved by Newton-Raphson iteration technique and is provided to update the initial guess of the dielectric constant ϵ_1.

$$|F'(\epsilon_1)| = \frac{|F(\epsilon_1 + \Delta)| - |F(\epsilon_1)|}{\Delta} \tag{2.22}$$

After the first iteration, the new guess value ϵ_2 is obtained from $\epsilon_2 = h + \epsilon_1$, and is substituted instead of ϵ_1 in Equation (2.21). As a result of the n^{th} iteration, Equation (2.23) is obtained similar to Equation (2.20).

$$\epsilon_{n+1} = \epsilon_n - \frac{F(\epsilon_n)}{F'(\epsilon_n)} \tag{2.23}$$

The stopping criterion is determined depending on the desired sensitivity and is checked whether the new obtained dielectric constant satisfies this criterion. Unless the stopping criterion is satisfied, iteration is continued. As soon as the criterion is satisfied, the result has been reached and an unknown dielectric constant has been obtained.

It was explained how to do iteration when measuring from one point. For the one point measurement, the update parameter can be calculate at one step easily. If the measurement is taken from k points to increase the sensitivity, the number of equations is higher than the number of unknown variables. Thus, the Least Squares Method is implemented since it is desired to get one update parameter using all measurement points (Bickel and Doksum, 2007). So the equation we need to solve becomes;

$$[A]^T [A] [h] = [A]^T [b] \tag{2.24}$$

where

$$A = \begin{bmatrix} |F'(\epsilon_1)|^{(1)} \\ |F'(\epsilon_1)|^{(2)} \\ \dots \\ \dots \\ |F'(\epsilon_1)|^{(k)} \end{bmatrix}_{k\times 1} \qquad b = \begin{bmatrix} |F(\epsilon_x)|^{(1)} - |F(\epsilon_1)|^{(1)} \\ |F(\epsilon_x)|^{(2)} - |F(\epsilon_1)|^{(2)} \\ \dots \\ \dots \\ |F(\epsilon_x)|^{(k)} - |F(\epsilon_1)|^{(k)} \end{bmatrix}_{k\times 1} \tag{2.25}$$

The matrix A contains the derivatives and the matrix b consists of differences. $[A]^T$ denotes the transpose of the matrix A. The h parameter is attained from these equations and the new dielectric constant to be used is decided and the next iteration is carried out.

2.4. Finite Element Method

Analytical analysis of complicated structures is often not possible. For this reason, numerical methods are used to solve many electromagnetic problems. In this thesis, it is planned to excite the cavity, observe the S-parameters, and read the electric field and power values using the CST-MWS program. There are many options such as finite element method (FEM), finite integration technique (FIT) offered by this program to users. Within the scope of this study, frequency domain solver using FEM is utilised.

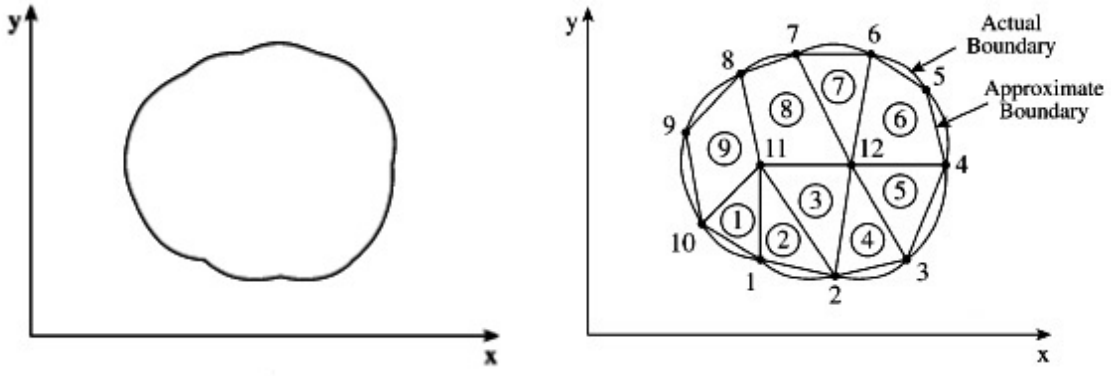

(a) (b)

Figure 2.4. FEM mesh structure (a) Without mesh (b) With mesh

FEM, which is used in modules such as eigenmode solver and frequency domain solver in CST-MWS software, has an important role in electromagnetics as in many other areas. In the finite element method, the problem region is divided into sub-sections called finite elements, and the electromagnetic problem is handled in this way. A problem can be solved with FEM in 4 main steps. First of all, the region must be divided into elements, that is discretization, see Figure 2.4 (Sadiku, 2000). Secondly, an appropriate interpolation function must be selected, then the formulation for the problem must be created and the corresponding equation system must be solved as the last step.

Discretization step is one of the most important steps of FEM. In this step, dividing the solution region into finite elements is performed. Finite elements can be tetrahedral or hexahedral according to the shape and dimensions of the structure, see Figure 2.5 (Sadiku, 2000). At this stage, discretization should be done very precisely. Therefore, in many problems that are handled by finite element method, meshing takes more time than the sum of all remaining processes.

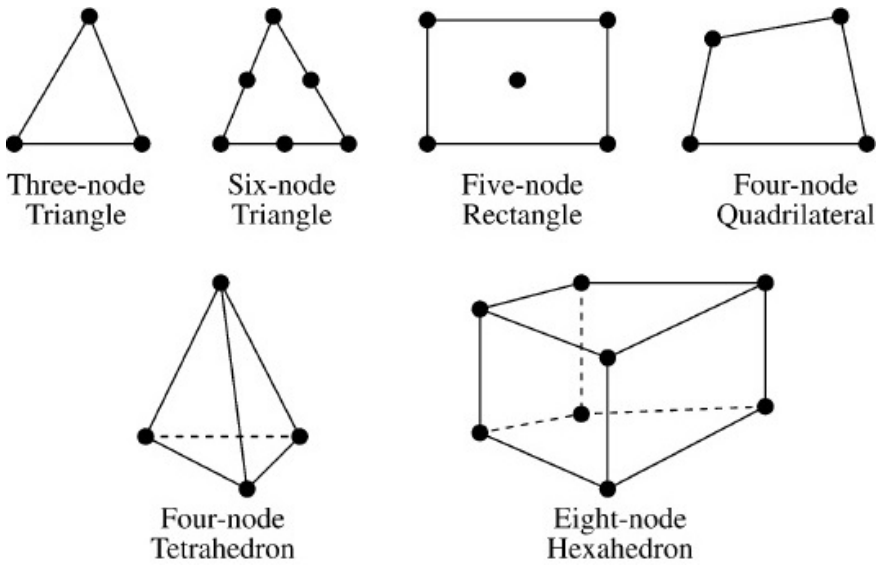

Figure 2.5. FEM mesh types for various 2D and 3D

In the second step, an approximation is selected for the solution of the electromagnetic problem. This approximation can be a polynomial or a sinusoidal function. If the selected function is a polynomial, the degree of the polynomial is directly related to the sensitivity of the solution.

In the third and fourth steps, the system of equations is created and solved, respectively. When creating the system of equations, defining boundary conditions appropriately

is an important part of the solution of the system. This system of equations can be solved with 2 different methods: iterative method or band matrix method (Sadiku, 2000). After the equation system is solved, the corresponding impedance values and S-parameters can be obtained easily.

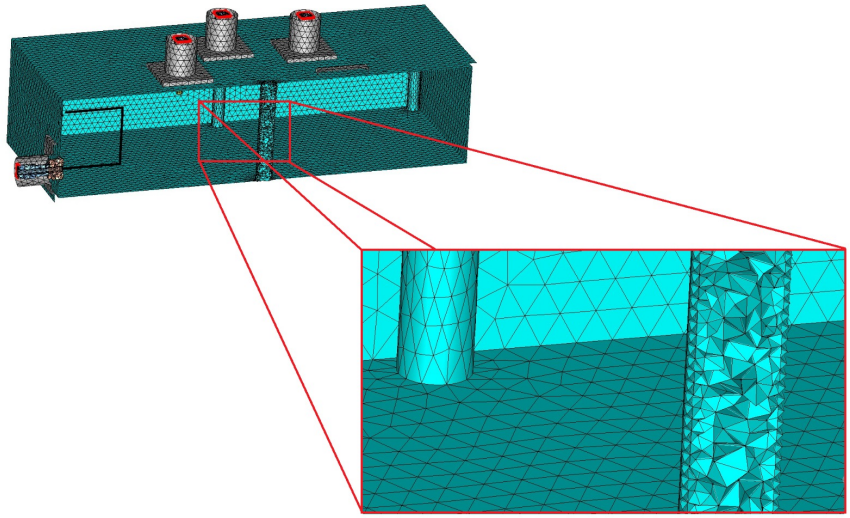

Figure 2.6. Tetrahedral mesh view in frequency domain solver of CST-MWS

As an example, the tetrahedral mesh structure of the CST-MWS software can be seen in Figure 2.6. The mesh structure in this figure corresponds to four-node tetrahedrons. As the number of mesh increases, precision is expected to improve. After reaching the particular number of mesh, the change in results converges to zero. In addition, with the adaptive mesh algorithm used by the CST-MWS program, regions with sudden changes will have smaller meshes.

CHAPTER 3

RESULTS OF MATERIAL PERTURBATION METHOD

This chapter is dedicated to the material perturbation approach in dielectric measurements. Rectangular and cylindrical cavities, which are frequently used in resonant methods, are compared with CST-MWS simulations. After that, dielectric constants of different materials are measured using a real cavity.

3.1. Rectangular and Cylindrical Cavity Comparison

The effect of the parameters in the dielectric constant equations and cavity shapes on dielectric measurements is studied numerically using the material perturbation method that emphasized the inverse problem analogy. The direct problem involves taking the measurement from the dielectric-loaded cavity and finding the resonant frequency for a defined dielectric constant. The idea of the inverse problem is to find the reconstructed dielectric constant value by recalculating the dielectric constant with the help of Equation (2.18) from the obtained frequency shift.

Microwave cavities resonate at a particular frequency corresponding to the certain mode. The resonant frequencies of the modes employed (TE_{101} and TM_{010}) are given for the rectangular and cylindrical cavity, respectively, in Equations (3.1) and (3.2). In the first equation, a and d shows the width and the length dimensions of the rectangular cavity. R stands for the radius of the cylindrical cavity in the other equation. χ_{01} demonstrates additionally the root of the Bessel function for TM_{010} mode.

$$f_{101}^{TE} = \frac{1}{2\sqrt{\epsilon\mu}}\sqrt{\frac{1}{a^2}+\frac{1}{d^2}} \tag{3.1}$$

$$f_{010}^{TM} = \frac{1}{2\pi\sqrt{\epsilon\mu}}\frac{\chi_{01}}{R} \tag{3.2}$$

The resonant frequency of the desired mode for the empty cavity, f_0 is determined as the reference value using the full-wave electromagnetic simulator CST-MWS and the previously mentioned Equation (2.18) is rewritten;

$$\epsilon_r = 1 + \xi \frac{V_c}{V_s} \frac{f_0 - f_s}{f_0} \tag{3.3}$$

where ϵ_r indicates the relative dielectric constant. As mentioned before, ξ is 0.5 for the rectangular cavity and 0.539 for the cylindrical cavity. V_c and V_s represent the volumes of the cavity and the sample respectively.

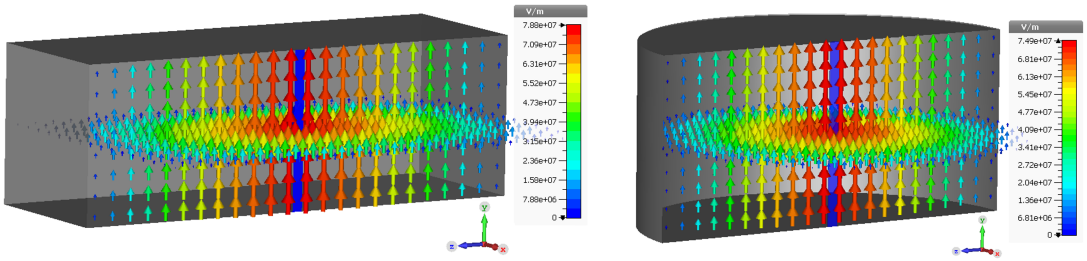

(a) (b)

Figure 3.1. E-field distributions (a) Rectangular cavity for TE_{101} mode (b) Cylindrical cavity for TM_{010} mode

Two investigations based on the comparison between rectangular and cylindrical cavities were performed (Ozkal and Yaman, 2019). In both cavities, the material under test is placed in the centre of the cavities. In accordance with this design, the TE_{101} mode in the rectangular cavity and the TM_{010} mode in the cylindrical cavity are excited. E-field distributions of the mentioned modes can be examined in Figure 3.1. The colour bars at the right of the figures belong to specific input power, and their numerical values change depending on the variation of the default power accepted to be transmitted to the system.

The first investigation focuses on how accuracy is disrupted by the increase in dielectric constant value for rectangular and cylindrical cavity shapes. Cavities are designed such that their volumes are approximately equal and also their chosen modes operate at the frequency of 3 GHz. Similarly, sample volumes keep the same value at each step, the ratios of cavity volumes to sample volumes are kept constant in this way. As a result, the

variables in Equation (3.3) are just frequency shift and relative dielectric constant. While the exact dielectric constant defined within the direct problem increases from 2 to 20, the error rate is calculated as follows;

$$error\ rate\ \% = \frac{|\epsilon_{exact} - \epsilon_{reconstructed}|}{\epsilon_{exact}} \times 100 \tag{3.4}$$

where $\epsilon_{reconstructed}$ shows the dielectric constant recalculated in the inverse problem.

Figure 3.2 demonstrates reconstructed dielectric constant values and error rates at each step while exact dielectric constant values rise. The Y data inside the boxes over the curves indicate outcomes for the rectangular cavity, while the boxes under the curves give the results of the cylindrical cavity.

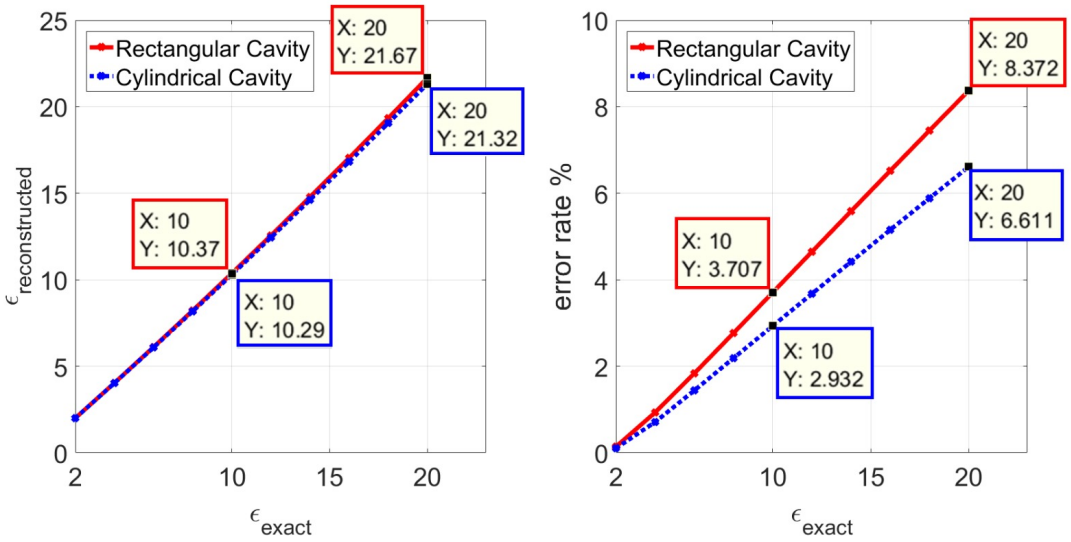

Figure 3.2. Reconstructed dielectric constant and error rate comparison at 3 GHz

The accuracy decreases with the increment in the dielectric constant value since the material perturbation method works for the minor changes. Observing the error rate graph to consider the difference between rectangular and cylindrical cavities more clearly, it is seen that the error rate of the rectangular cavity reaches to greater values.

The second investigation examines how the reconstructed dielectric constant value is affected if the resonant frequency for the empty cavity and the sample volume, which was held constant in the previous case, changes. The volumes of the cavities are reduced

to increase the resonant frequencies of the cavities, but the rectangular and cylindrical cavities for each step are designed so that their volumes are almost the same. The investigation is carried out for 2 different dielectric constants, 5 and 10. Sample volumes are decided for 3 cases; 50, 200 and 800 mm^3 and S-band is preferred as the frequency range. While the resonant frequency of the TM_{010} mode of the cylindrical cavity is determined only by the radius of the cylinder, there are limitations for the rectangular cavity, since 2 dimensions are required for the TE_{101} mode. For these reasons, analyzes are carried out in 2 consecutive frequency ranges, 2-3 GHz and 3-4 GHz.

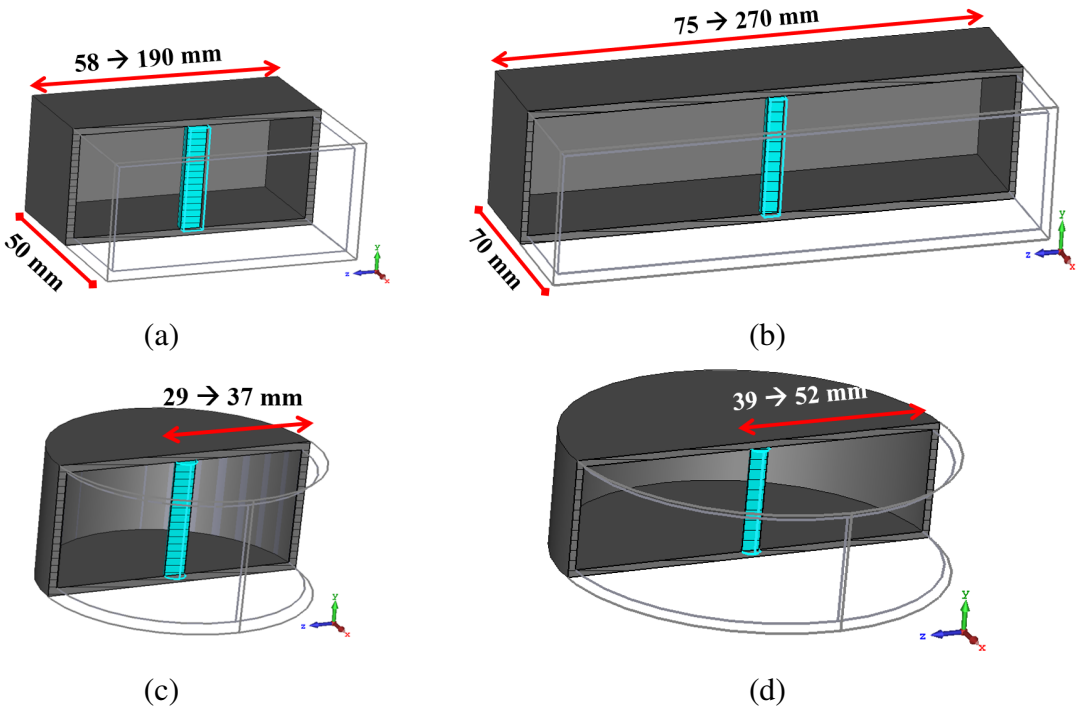

Figure 3.3. Cavity dimensions for comparison (a) Rectangular cavity for 4-3 GHz (b) Rectangular cavity for 3-2 GHz (c) Cylindrical cavity for 4-3 GHz (d) Cylindrical cavity for 3-2 GHz

As seen in Figure 3.3, the cavities' dimensions are risen to decline the frequency for two frequency range. In accordance with the modes, the samples are located where the electric field has the highest magnitude at each time.

Figure 3.4 presents the comparison results for the rectangular cavity (3.4.a and 3.4.c) and the cylindrical cavity (3.4.b and 3.4.d) using the sample with dielectric constant 5 via material perturbation theory. The frequency range of 2-3 GHz is stated in Figure 3.4.a and 3.4.b, while the frequency range of 3-4 GHz is expressed in Figure 3.4.c

and 3.4.d. As the frequency increases, the error rate decreases in the rectangular cavity simulations, whereas the cylindrical cavity has the contrary behaviour and its inaccuracy rises. When the sample volume is very small, the error rate is around 1%. As expected, the error grows quickly as the sample volume is at its greatest value, since the perturbation approach is not satisfied. Looking at the results of the rectangular cavity, a sudden increment is noticed at around 3 GHz in the transitions of the frequency range because the dimensions modify.

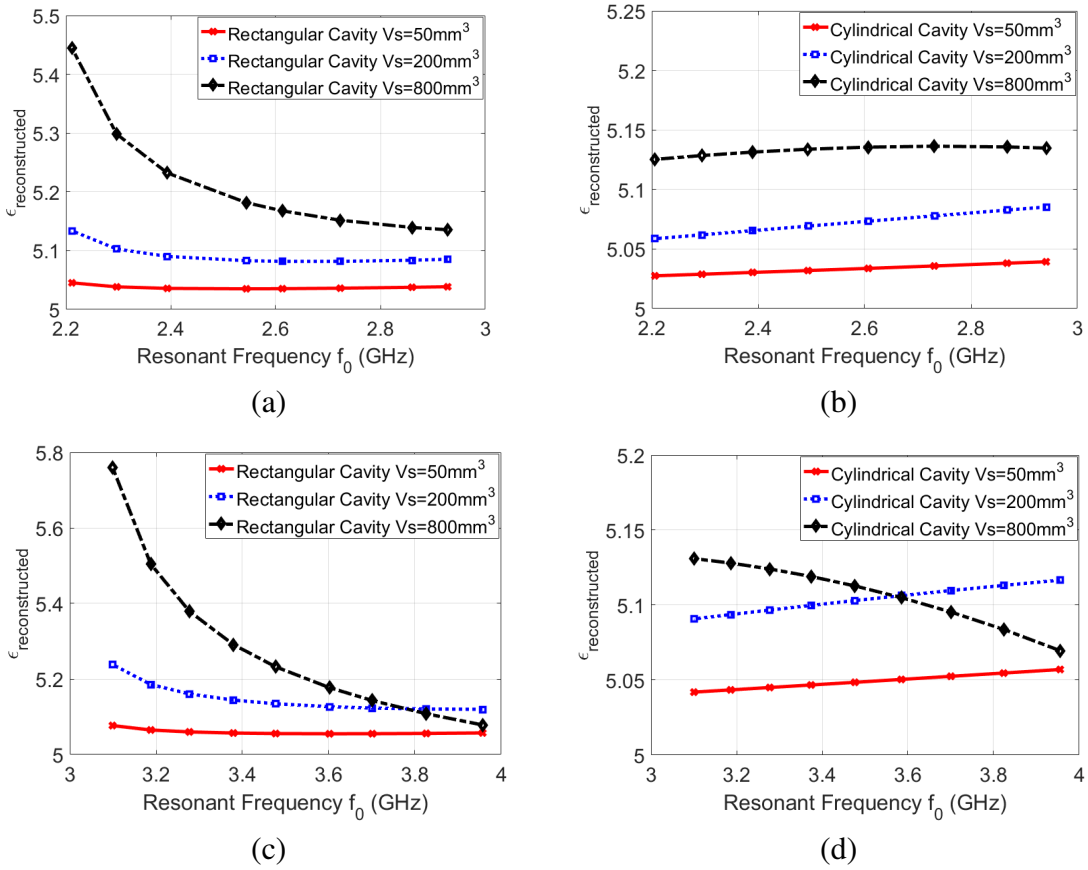

Figure 3.4. Reconstructed dielectric constant comparison for varying volume of sample with $\epsilon_r = 5$ (a) Rectangular cavity for 2-3 GHz (b) Cylindrical cavity for 2-3 GHz (c) Rectangular cavity for 3-4 GHz (d) Cylindrical cavity for 3-4 GHz

When the dielectric constant 10 is selected, the cavities present the same behaviour; however, as it will be deducted from the first investigation, the precision decreases due to the increase in the dielectric constant value as shown in Figure 3.5. When Figure 3.5.c is examined for the rectangular cavity, it is determined that the error rate at

the frequency of 3.1 GHz rises to 40%, and this is the worst case of the rectangular cavity. The reason for the error rate to behave differently when using a cylindrical cavity in case the sample volume is 800 mm^3 is that the ratio of the cavity volume to the sample volume is very low.

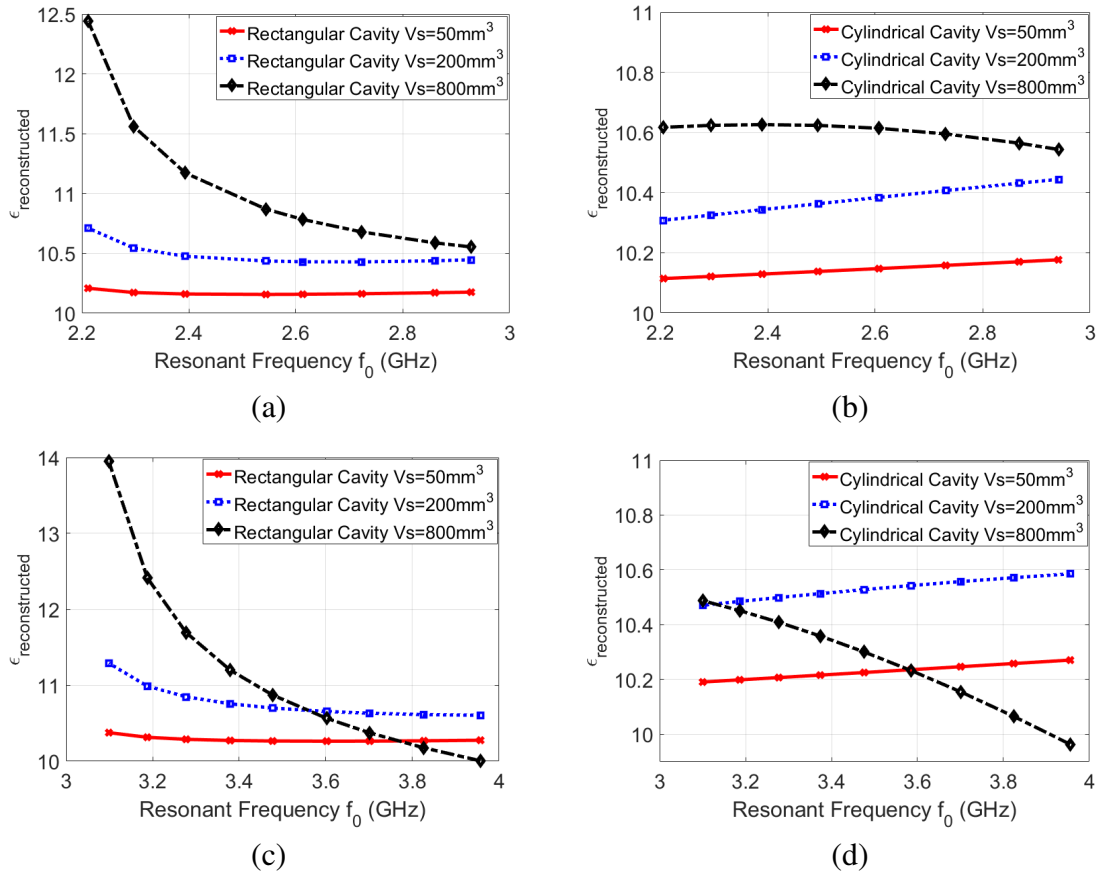

Figure 3.5. Reconstructed dielectric constant comparison for varying volume of sample with $\epsilon_r = 10$ (a) Rectangular cavity for 2-3 GHz (b) Cylindrical cavity for 2-3 GHz (c) Rectangular cavity for 3-4 GHz (d) Cylindrical cavity for 3-4 GHz

In general, high frequencies in rectangular cavities and low frequencies in cylindrical cavities should be preferred. High sample volume causes higher errors in material perturbation theory for almost all cases. Although the error rate in the cylindrical cavity is low, it either tends to increase continuously or decrease continuously, giving remarkably unstable results. However, as the frequency increases in the rectangular cavity, more stable results are obtained.

3.2. Measurement Results of the Perturbation Method

The material perturbation approach was implemented using a real cavity with different materials. An aluminum rectangular box was bought and turned into a cavity by providing suitable connector holes. The bought cavity (see Figure 3.6) was drawn identically in CST-MWS.

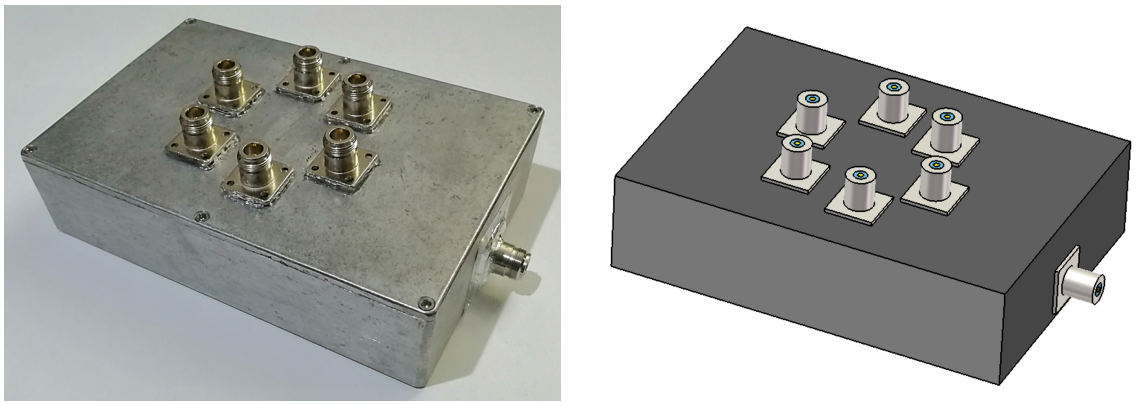

(a) (b)

Figure 3.6. Cavity Design (a) Real Cavity (b) Drawn cavity in CST-MWS

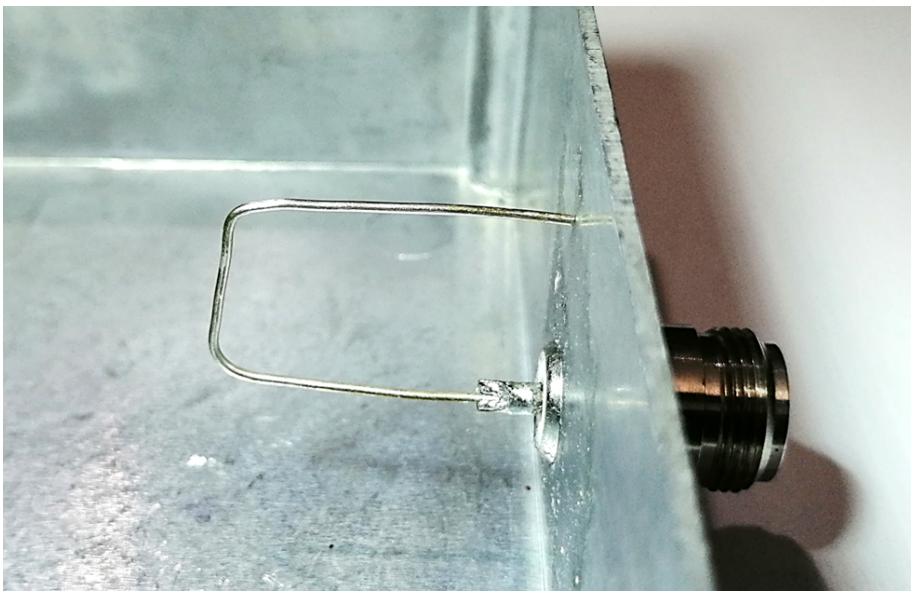

Figure 3.7. Coupling loop exciting the cavity

In previous studies (Ozkal and Yaman, 2018), we presented that measurements were taken only when one connector was attached to the cavity. In this thesis, six connectors were placed on the cover of the cavity and the measurement was taken again. Since the same conditions were provided in the reference and sample measurements, the results were determined to be compatible with each other. Six connectors placed on the top of the cavity will be utilised in the section of the results of the Newton-Raphson method. Reflection parameter (S_{11}) was examined by using only the connector on the sidewall in the material perturbation method.

The cavities must be coupled with the transmission lines to transfer power. Coupling is generally provided in three ways as hole, probe and loop (Balanis, 2012). If the waveguide will be used as the transmission line, the hole is utilised. When the coaxial line is preferred as the transmission line, the probe is employed for excitation from the electric field region and the loop from the magnetic field region (Pozar, 2012). In the case of magnetic coupling, the inner conductor of the coaxial line is terminated with the short circuit to the cavity wall. The current flowing through the magnetic loop induces a magnetic field perpendicular to the plane of the loop. As seen in Figure 3.7, the coupling loop was utilised for this study. A connector and a loop antenna were put to transfer power into the cavity from the narrower sidewall of the cavity.

Figure 3.8. Filled glass tube and screw holes of the cavity

For the measurement of liquid samples, the tube which the sample was filled was selected from the glass. The glass tube was pasted to the bottom of the cavity with hot

silicone (see Figure 3.8). The dielectric constant of the glass is about 4.8, and that of the silicon is about 11.9 at room temperature in the literature (CST MICROWAVE STUDIO, 2018). However, the measurement results were not affected, since the contribution of glass and silicon was at every measurement and empty glass tube condition was decided as the initial reference value. Screw holes used to fix the cavity cover can be also seen from Figure 3.8.

The measurement setup where the material perturbation approach was performed is displayed in Figure 3.9. After the one-port calibration of the VNA was done in the appropriate frequency range, the reflection parameter S_{11} of the cavity was measured and the data collected were plotted through the PC.

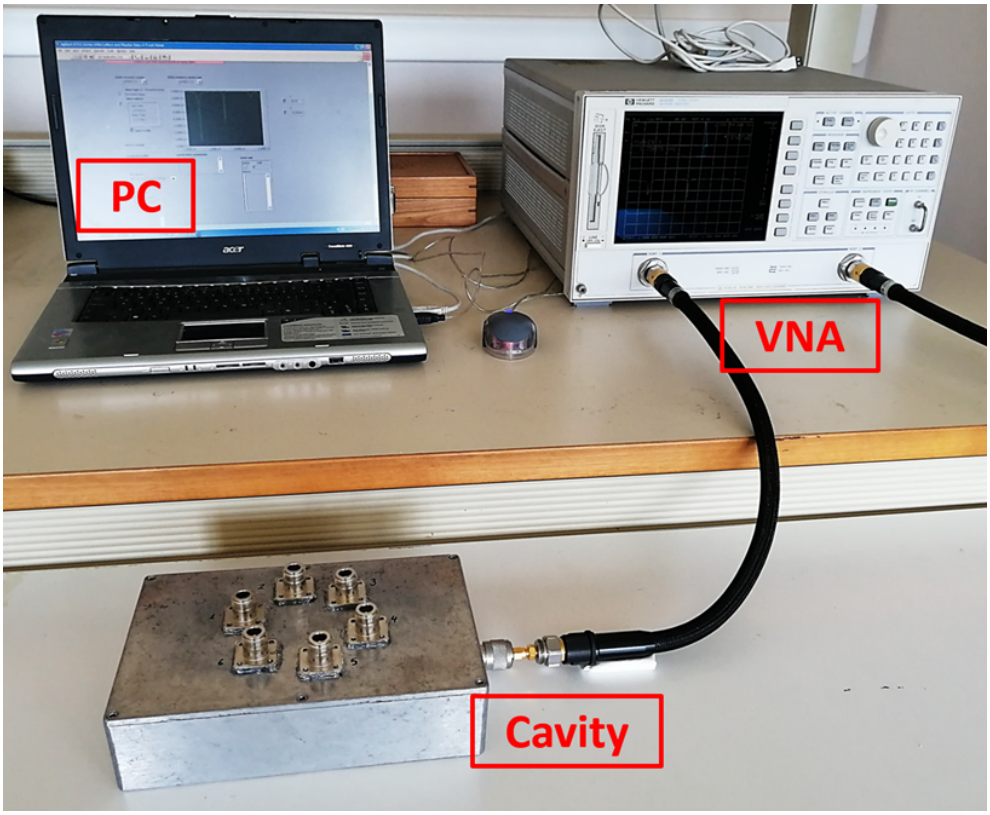

Figure 3.9. Material perturbation method measurement setup

The reference value needed to determine the frequency shift for the material perturbation approach was obtained in the case of the empty glass tube inside the cavity. The same condition was simulated in CST-MWS and the S_{11} matching seen in Figure 3.10 was obtained. The dotted blue line shows the measurement result with VNA, and the dashed red line gives the CST-MWS simulation result.

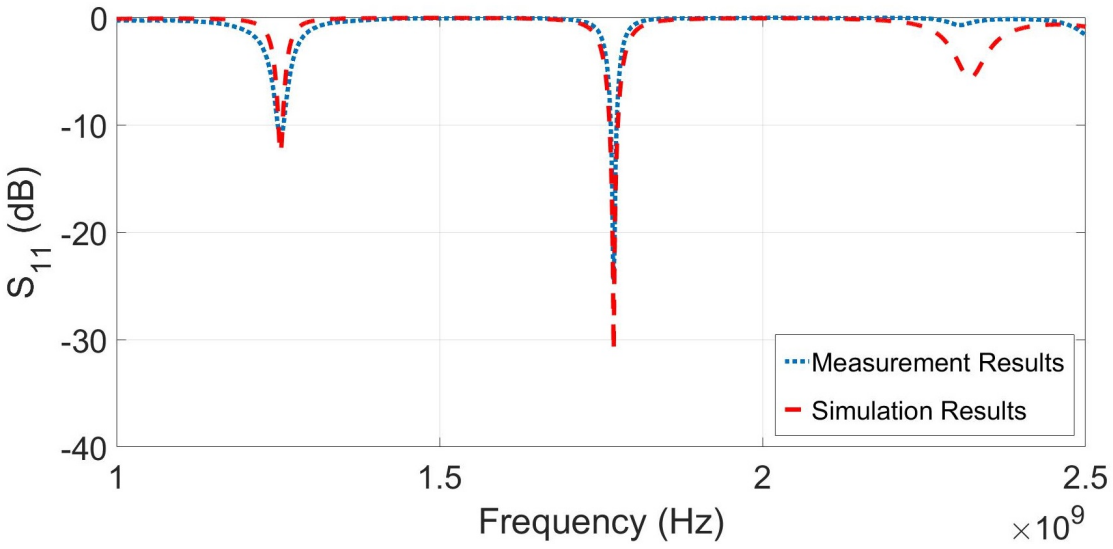

Figure 3.10. S_{11} results of the empty cavity

Within the scope of this thesis, measurements were performed for 3 samples with low, medium and high dielectric constant values. Firstly, the frequency in the case of an empty glass tube inside the cavity was determined as the reference value. Then measurements were carried out for hexane, ethanol and drinking water, which were easily available. The ethanol used in the experiments contains 4% water and is expressed as ethanol 96%.

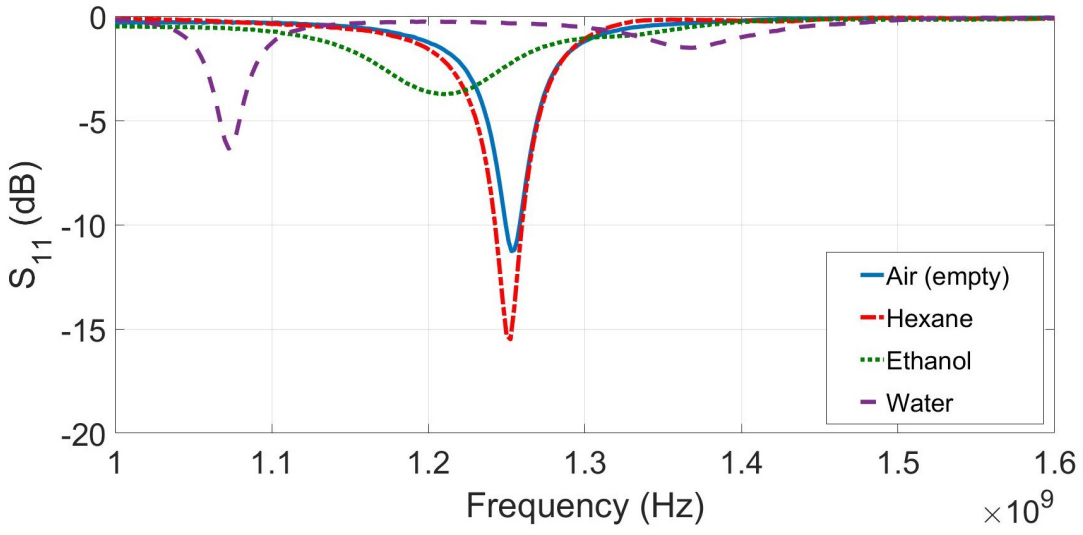

Figure 3.11. Material perturbation measurement results

The results obtained from VNA with frequency shift when hexane, ethanol-water mixture and drinking water are filled into the glass tube are given in Figure 3.11. The blue line is the result of the empty case given in Figure 3.10 from the VNA.

Since the hexane's dielectric constant is small, the frequency shift is more invisible. However, the dielectric constant of drinking water is high, so there has been a greater shift in frequency.

Table 3.1. Material perturbation approach for various liquid samples

	Hexane	Ethanol 96%	Water
$\epsilon_{reconstructed}$	1.71	13.73	52.21
$\epsilon_{literature}$	1.89	16.64	71.7
$error\ rate$	9.52%	17.49%	27.18%

Reconstructed dielectric constant results given in Table 3.1 were obtained by including cavity and sample volumes in Equation (3.3) as in the comparison of cavities. Also, dielectric constant values in the literature for hexane, ethanol 96% and drinking water were written (Hayakawa and Sawa, 1997 ; Abdelgwad and Said, 2015). However, since the ethanol used in the experiment is water-added, the dielectric constant is calculated according to the water content after it is obtained from the literature according to the operating frequency (Sato and Buchner, 2004 ; Puvvadi et al., 2008). The error rate for hexane is around 9.52% and for ethanol is almost 17.49%. For drinking water, around 27.18% error occurred. Perturbation approach fails at the high dielectric constant of the water, as it is responsive to minor changes. Due to the fact that the dielectric constant of the water is the divergence from the perturbation approach, it is an expected situation with the results in the comparison of the cavities. The error rate increased as the dielectric constant raised.

Measurements were also performed for different concentration levels of ethanol. Half of the glass tube was filled with ethanol 96% and the other half with distilled water. Because of equal volumes, ethanol was 48%, the dielectric constant was calculated as 48.32. Ethanol 96% and distilled water were mixed with the ratio 2:1 to obtain ethanol 64%. The dielectric constant of the new mixture was calculated as 37.76.

As the amount of ethanol increases in the mixtures, the dielectric constant is lower. Table 3.2 represents the reconstructed dielectric constants with various concentration lev-

els of ethanol. As with previous measurements, the error rate increases as the dielectric constant becomes higher.

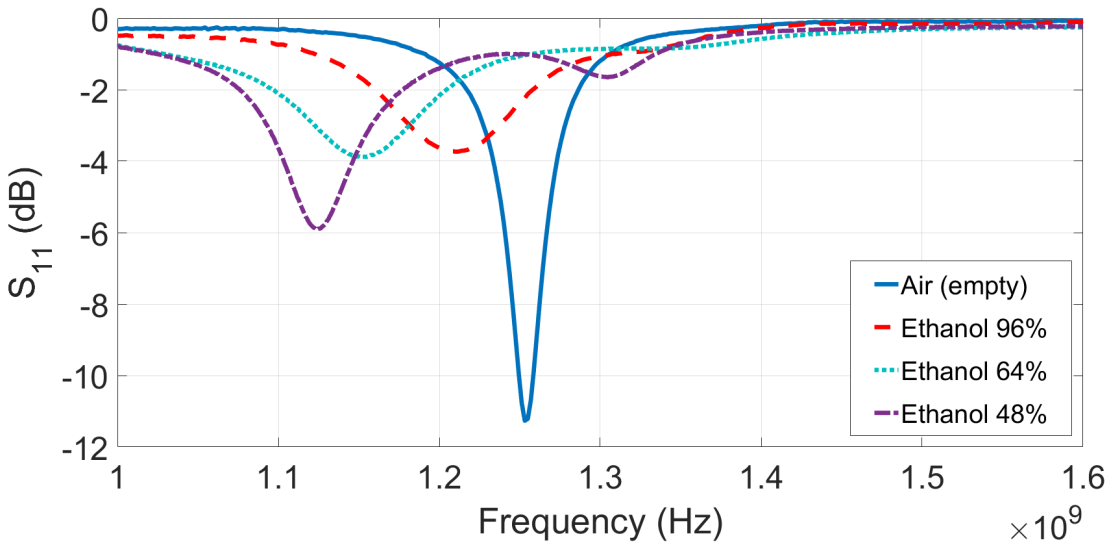

Figure 3.12. Material perturbation results for different concentration of ethanol

Table 3.2. Material perturbation approach for various ethanol concentrations

	Ethanol 96%	Ethanol 64%	Ethanol 48%
$\epsilon_{reconstructed}$	13.73	30.003	37.92
$\epsilon_{literature}$	16.64	37.76	48.32
$error\ rate$	17.49%	20.54%	21.52%

The reasons for the inaccurate results for low dielectric constants may be the roughness on the inner surface of the cavity and the material of the cavity being lower conductivity aluminium. In addition, dielectric and cable losses during measurement can cause erroneous results. The Newton-Raphson approach will be presented in the next chapter to obtain more accurate results for materials with a higher dielectric constant.

CHAPTER 4

RESULTS OF NEWTON-RAPHSON METHOD

The applicability of the Newton-Raphson method to the dielectric measurements with a rectangular cavity has been demonstrated by simulation via CST-MWS using electric field values. Then, the power values were measured using a spectrum analyzer and the method was verified by measurements.

4.1. Simulation Results of the Newton-Raphson Method

The aluminium rectangular cavity was designed in CST-MWS, which can be seen in Figure 4.1. Power was supplied to the cavity with a loop antenna. A glass tube was placed in the middle of the cavity and is filled with the material under test. The electric field values were examined on the curve drawn around it.

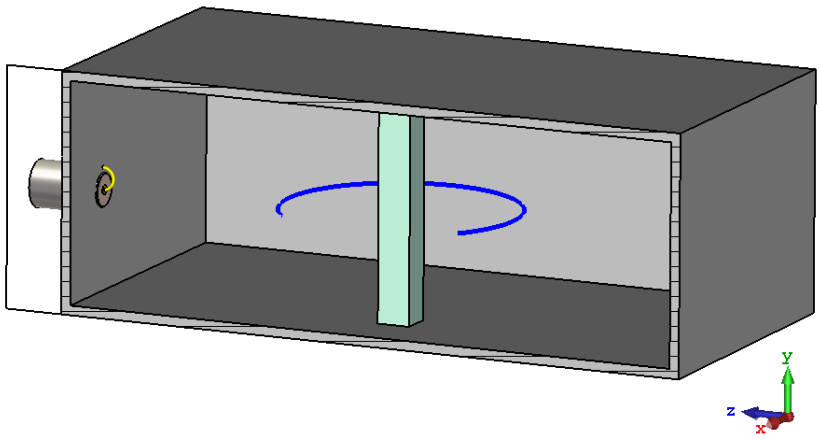

Figure 4.1. Cavity design in CST-MWS with a curve around the sample

The process was performed by selecting 32 values at certain intervals from the electric field values. Since any mode is not excited, the electric field values are at low levels, and the electric field distributions for the cavity with empty glass tube are presented in Figure 4.2. As the mode of a particular frequency is not produced, the effect of the modes near the frequency used can be seen. The curve drawn around the tube is shown

with red colour and also the electric field amplitudes are normalized by 50 to become the field distribution more understandable.

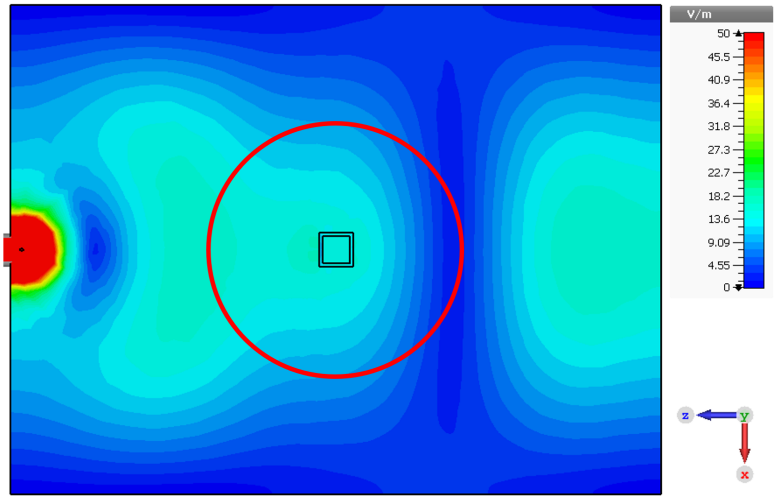

Figure 4.2. Electric field distributions in 3D with empty glass tube at 2.6 GHz

The distribution of the modes near the frequency of 2.6 GHz can be seen in Figure 4.4 when there is a sample with dielectric constants of 10, 20, 30, 40 and 50. The 3D distribution of the electric field can also be examined from Figure 4.3 for two materials with the dielectric constants of 10 and 50.

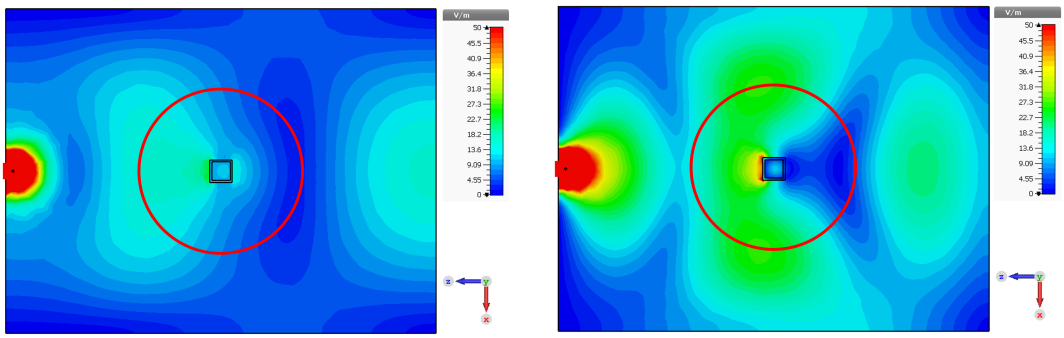

(a) (b)

Figure 4.3. Electric field distributions in 3D inside the cavity at 2.6 GHz (a) Dielectric constant of 10 (b) Dielectric constant of 50

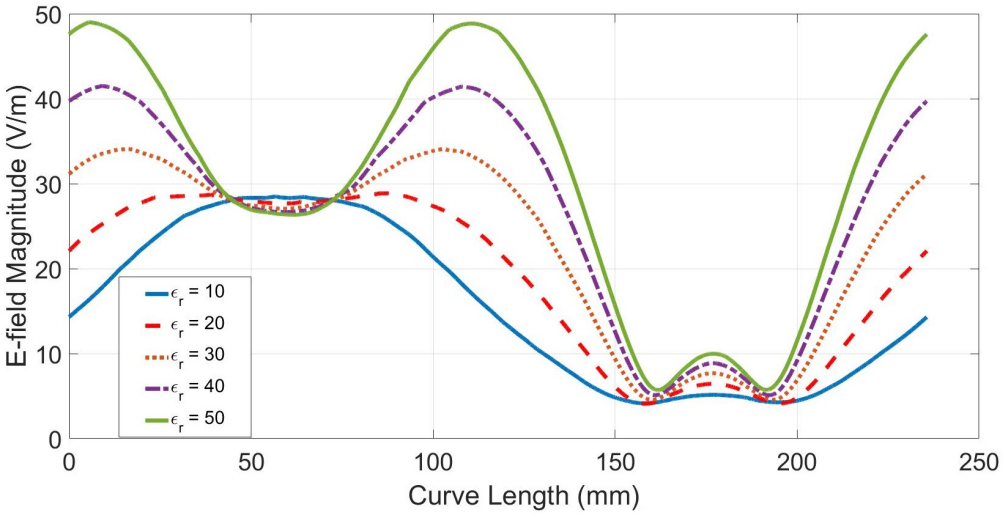

Figure 4.4. Electric field distributions in 1D on the curve

Let's give an example calculation in the application of the Newton-Raphson method to the dielectric measurements. If the dielectric constant of the sample whose electrical properties are not known is ϵ_x (ϵ_x is unknown), then the magnitude of the measured electric field values of that sample are shown with $E(\epsilon_x)$. In other words, if our ϵ_x value is equal to 50, then the point of 50 is tried to reach with the iteration approach. Let's assume that we have another material that can be used as an initial point whose dielectric constant is 20 ($\epsilon_1 = 20$) and $E(\epsilon_1 = 20)$ indicates the obtained electric field magnitude values of the reference material. Our main aim is to approach the dielectric constant of the unknown material by starting the iteration from 20. If our Δ value is 1, which indicates the steps, we also need the electric field values obtained from the simulation and occurred when the dielectric constant is 21. The next iteration value ϵ_2 is calculated as specified in Equation (4.1). Thus, ϵ_x values are achieved by using $\epsilon_{2,3...(x-1)}$ values, as explained before, with stopping criterion.

$$\epsilon_2 = 20 - \frac{E(\epsilon = 20)\Delta}{E(\epsilon = 21) - E(\epsilon = 20)} \qquad where \qquad \epsilon_2 = \epsilon_1 + h \tag{4.1}$$

Newton-Raphson method simulations were analysed in terms of 3 different variables as the difference quotient Δ, the initial guess ϵ_1 and the desired value to be reached ϵ_x. Iteration was stopped when the h value reached 10^{-3}, which is the stopping criterion.

The first examination was started with a material with the dielectric constant of

45, in other words, initial guess 45 was accepted. The sample with a dielectric constant of 50 is considered to be the material under test and it is assumed that the electric field values are measured. Iterations were performed by determining the difference quotient Δ as 0.1, 0.5, 1 and 3. The obtained results $\epsilon_{1,2...x}$ and update parameter h, is given in Table 4.1 and shown graphically in Figure 4.5.

Table 4.1. Newton-Raphson simulations from 45 to 50 with various Δ values

#	$\epsilon_\mathbf{r}$ Δ=0.1	h Δ=0.1	$\epsilon_\mathbf{r}$ Δ=0.5	h Δ=0.5	$\epsilon_\mathbf{r}$ Δ=1	h Δ=1	$\epsilon_\mathbf{r}$ Δ=3	h Δ=3
0	45	2.577	45	3.744	45	4.9579	45	4.9567
1	47.577	1.7523	48.744	0.732	49.9579	0.1166	49.9567	0.1146
2	49.3293	0.4581	49.476	0.4086	50.0745	0.0202	50.0713	0.0026
3	49.7874	0.1888	49.8846	0.0893	50.0947	-0.0159	-	-
4	49.9762	0.0711	49.9739	0.068	50.0788	-0.0098	-	-
5	50.0473	-0.0305	50.0419	-0.0167	50.069	-0.0011	-	-
6	50.0168	0.0118	50.0252	0.0019	-	-	-	-
7	50.0286	-0.0034	-	-	-	-	-	-

As the Δ value increased, the desired value was reached faster because the step interval is wider. For the same reason, as iteration continues with tiny oscillations in narrower steps, final points closer to ϵ_x are achieved. Thus, the error rate is lower in small Δ values.

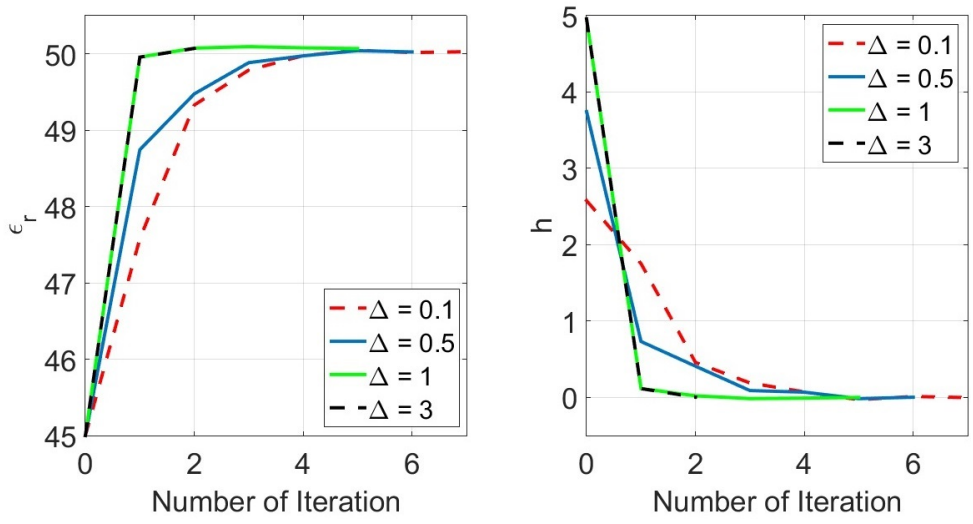

Figure 4.5. Simulations graphics of ϵ_r and h with various Δ values

In the second analysis, the effect of initial guess was observed. The desired value to be reached was decided 50 again and the Δ value was fixed to 0,1. Initial guess values were determined to be 10 and 30, thus attempting to reach from 10 and 30 to 50.

The h and ϵ_x values received in the iteration steps are given in Table 4.2 and Figure 4.6. The distance of the initial guess value from the final point does not have a major impact on accuracy. At this point, we note that the Newton-Raphson provides accurate numerical results based on good initial guesses. No matter how high the dielectric constant is, according to the observed parameters, it is clear that the Newton-type approach works.

Table 4.2. Newton-Raphson simulations with various initial points at $\Delta = 0.1$

#	ϵ_r ($\epsilon_1 = 10$)	h ($\epsilon_1 = 10$)	ϵ_r ($\epsilon_1 = 30$)	h ($\epsilon_1 = 30$)
0	10	33.2781	30	12.3062
1	43.2781	4.4065	42.3062	4.5906
2	47.6846	1.5294	46.8968	1.8528
3	49.214	0.5002	48.7496	0.8018
4	49.7142	0.245	49.5514	0.3057
5	49.9592	0.061	49.8571	0.1316
6	50.0202	0.0523	49.9887	0.0774
7	50.0725	0.0104	50.0661	-0.0286
8	50.0829	0.0033	50.0375	0.0173
9	-	-	50.0548	-0.0027

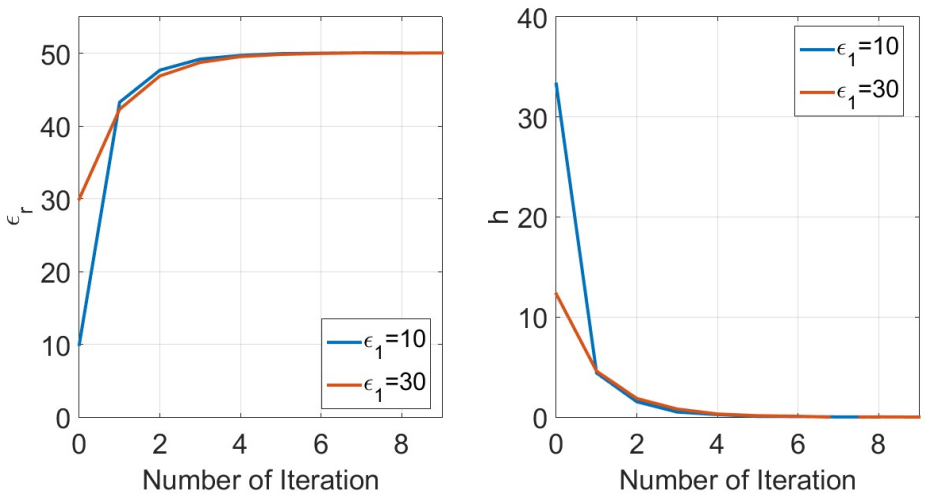

Figure 4.6. Simulations graphics of ϵ_r and h with various initial point values

In the last study, the Δ value was chosen as 1 and the initial guess was accepted as 10. The final point was determined as 3 different values and the method was applied to reach from 10 to 20, 30 and 40. Thus, while there is a material that we know the dielectric constant, the applicability of this method was examined in order to define the dielectric parameter of all other samples.

Table 4.3. Newton-Raphson simulations with various dielectric constants atΔ=1

#	$\epsilon_{\mathbf{r}}$ (ϵ_x=20)	h (ϵ_x=20)	$\epsilon_{\mathbf{r}}$ (ϵ_x=30)	h (ϵ_x=30)	$\epsilon_{\mathbf{r}}$ (ϵ_x=40)	h (ϵ_x=40)
0	10	14.6981	10	31.9349	10	48.167
1	24.6981	-4.7293	41.9349	-12.2866	58.167	-18.5988
2	19.9688	0.0762	29.6483	0.3351	39.5682	0.3784
3	20.045	0.0243	29.9834	0.0462	39.9466	-0.0055
4	20.0693	-0.0083	30.0296	0.0027	-	-
5	20.061	-0.0052	-	-	-	-

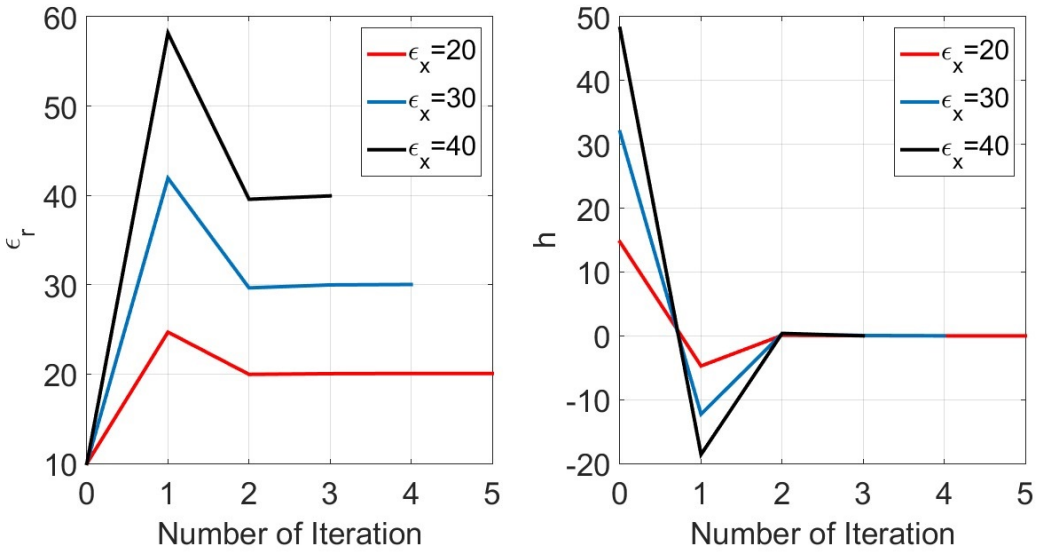

Figure 4.7. Simulations graphics of ϵ_r and h with various dielectric constant values

The results are written in Table 4.3 and shown in Figure 4.7. The reason for the sudden changes in the first iteration seen from the graphics is the high Δ value. The

dielectric constants of other samples could be reached with a single reference value, and the large Δ value provided a low number of iterations.

4.2. Measurement Results of the Newton-Raphson Method

The utilisation of the Newton-Raphson method in the dielectric measurements was performed using an aluminium rectangular cavity as shown in Figure 3.6.a after the simulation examination. Electric field values were obtained at 32 points in the simulation, and the power values were measured at 6 points in this investigation due to the size of the cavities and connectors. In the previous section, the design of the cavity in CST-MWS and the S_{11} matching (see Figure 3.10) for the empty cavity were mentioned.

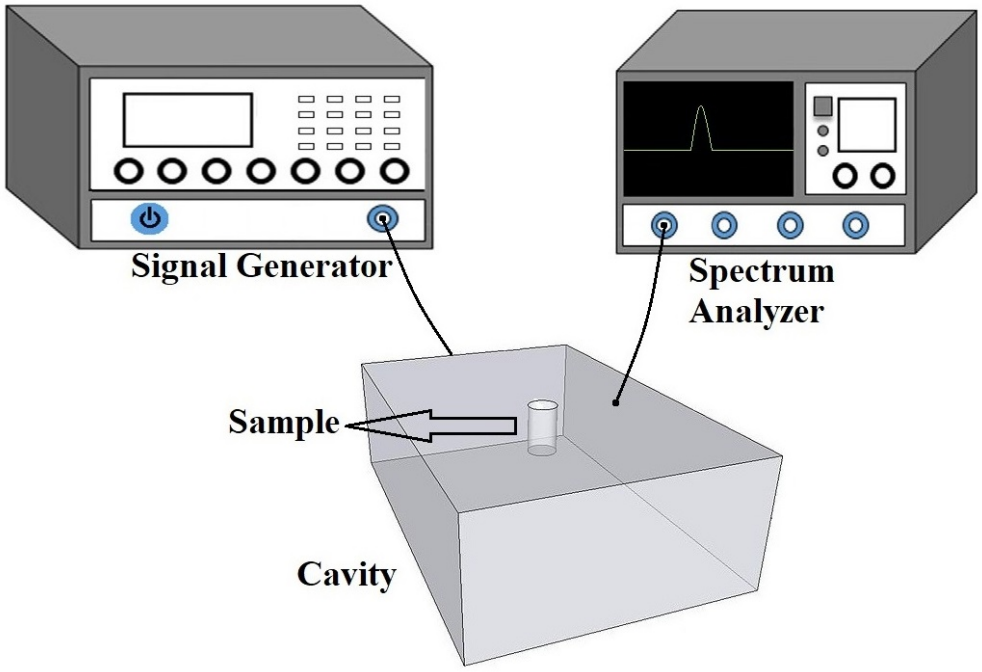

Figure 4.8. The illustration of the Newton-Raphson method measurement setup

The setup used in dielectric measurements with the Newton-Raphson method is presented in Figure 4.8. Power is transferred from the signal generator to the cavity at the specified frequency. The magnitude of the output power versus the same frequency is measured separately from the spectrum analyzer for each port. Iteration is performed on the simulation with the received power values.

The photo of the connectors from inside the cover of the cavity is given in Figure 4.9. No additional antennas were placed to ends of the connectors to form a probe antenna because the proximity of the antennas would cause them to be coupled to each other. For this reason, the inner conductors of the connectors, which extend out, were left to act as antennas.

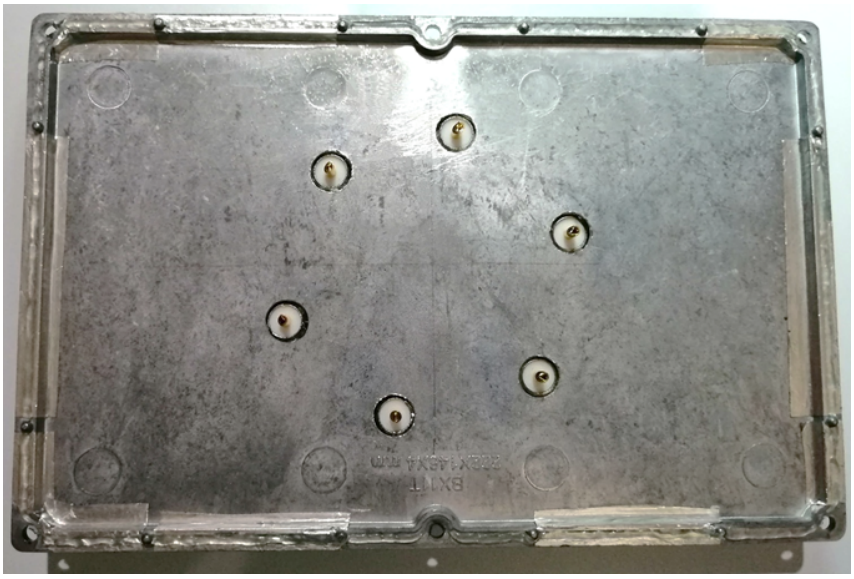

Figure 4.9. Photo of the cavity cover from the inside

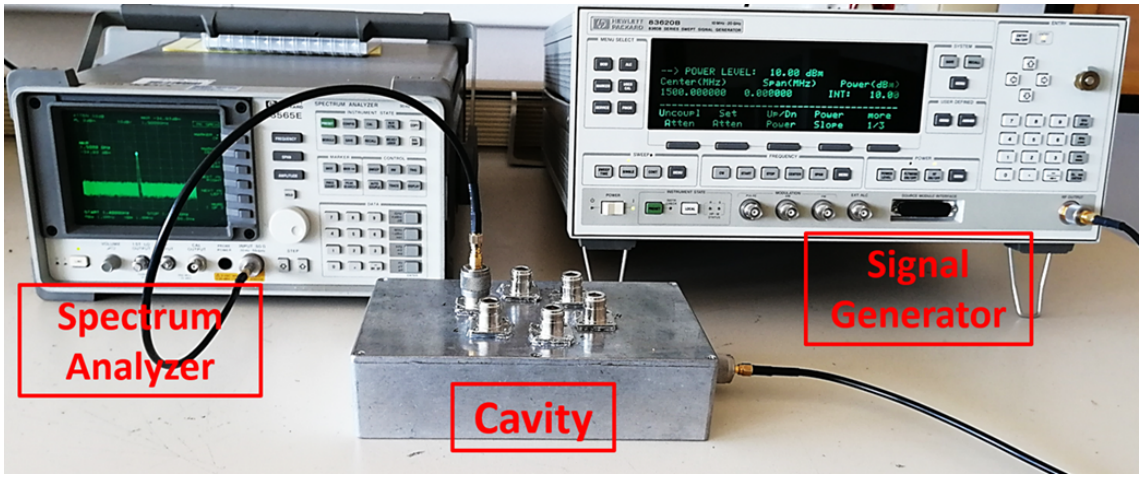

Figure 4.10. Newton-Raphson method measurement setup

Power measurement was carried out in the laboratory with the setup shown in Figure 4.10. 10 dBm of power was transferred to the cavity at a frequency of 1.5 GHz with the signal generator. The screenshot of the signal generator can be observed in Figure 4.11. The power value corresponding to the same frequency from the spectrum analyzer was measured individually for each port. Cables were chosen as short as possible to reduce cable loss.

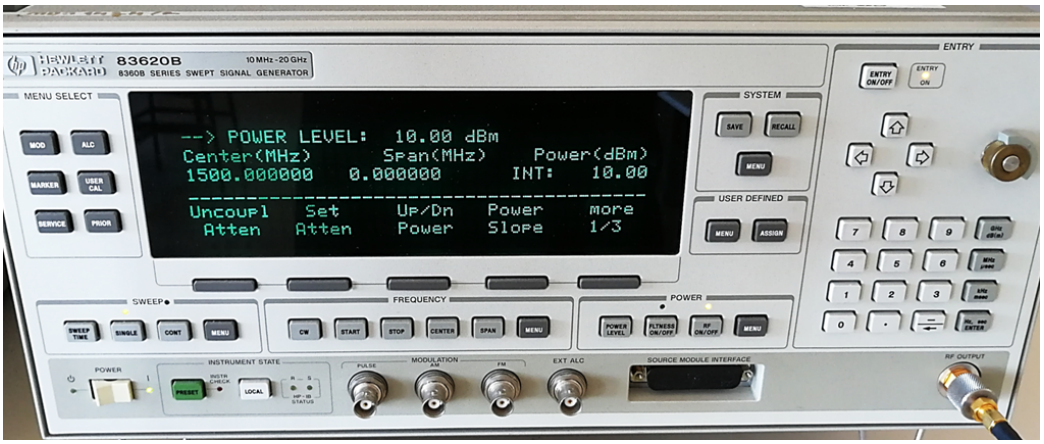

Figure 4.11. Signal generator screen

The system was calibrated with the empty cavity before proceeding to measure with the samples. The measurement results of the empty cavity at the spectrum analyzer and the power values received from CST-MWS were compared in Table 4.4 and normalization constants were calculated. These constants were added to the measurement results of the samples.

Table 4.4. Power measurements of the empty cavity case

	Port 1	Port 2	Port 3	Port 4	Port 5	Port 6
Power at CST-MWS (dBm)	-49.25	-47.46	-38.95	-36.83	-42.01	-58.19
Power at SA (dBm)	-48.83	-44.5	-37	-35.17	-40.33	-53.33
Normalization constant (dB)	0.42	2.96	1.95	1.66	1.68	4.86

Calibration was necessary since the original cavity have the rough inner surface and screw holes for the cover. The normalization constant was caused by the fact that there were millimetre position differences between the locations where the connectors were attached and the measurements points from the designed cavity in CST-MWS. Also, in real measurements, the connectors were pasted to the cavity with hot silicone so that some minor shifts at positions of the connectors occurred. For this reason, each port was calibrated with its own normalization constant.

Table 4.5. Power measurements of samples with the spectrum analyzer

	Port 1	Port 2	Port 3	Port 4	Port 5	Port 6
Hexane	-48.5	-44.67	-37.17	-35.33	-40.5	-54
Ethanol 96%	-43.67	-47.67	-39	-37.17	-42.5	-55
Ethanol 64%	-41.33	-61.83	-41.33	-39.17	-46.17	-44.67
Ethanol 48%	-40	-64	-43.17	-40.5	-49	-46.17
Drinking Water	-37.67	-58.17	-49.17	-45.83	-60.17	-48.5

In the implementation of the Newton-Raphson method with measurement, the empty cavity case was assumed as the initial guess and the value of ϵ_1 is 1 as the dielectric constant of the air. Hexane, water-added ethanol and drinking water which were measured in the material perturbation method were decided to be tested samples, and the desired points ϵ_x were the dielectric constants of these samples. In addition, the before mentioned samples with different dielectric constants obtained with various concentration levels of ethanol were also used in the measurements. Iterations were performed for two values of Δ as 1 and 0.1. The power measurement values for hexane, water-added ethanols and drinking water were presented in Table 4.5. Newton-Raphson iterations started with measurement results and continued on CST-MWS simulations.

To be an example of the measurements taken from the spectrum analyzer, the photo of the device screen is shared in Figure 4.12. In Figure 4.12.a and 4.12.b, in the case of the empty glass tube, power values received from ports 3 and 4 are displayed. The power values at port 3 and 4 can be read from Figure 4.12.c and 4.12.d when the glass tube is filled with water.

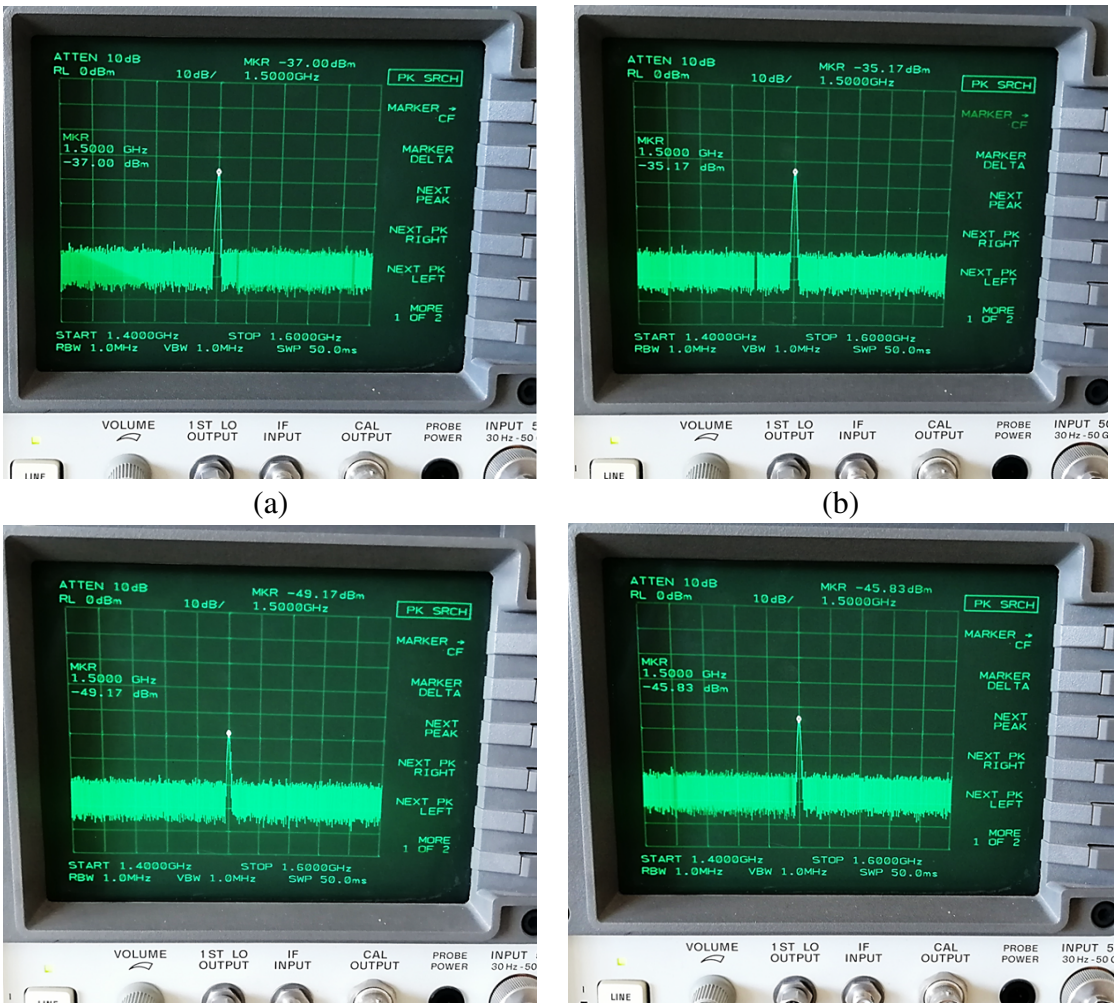

Figure 4.12. Power measurements on the spectrum analyzer screen (a) Empty cavity - port 3 (b) Empty cavity - port 4 (c) Water measurement - port 3 (d) Water measurement - port 4

In Table 4.6 and Figure 4.13, Newton-Raphson iteration results for hexane from the initial point of 1 can be seen. The reconstructed dielectric constant and the change of the update parameters were both plotted and tabulated. After each update parameter was calculated, it was added to the previous reconstructed dielectric constant as mentioned previously, and the new value was obtained and iteration continued.

The dielectric constant of hexane in the literature is 1.89, and 1.71 was detected by the material perturbation method. In the Newton-Raphson method, the reconstructed value approximates to 1.8653 for the step size of 1 and to 1.8691 when the step size is 0.1. The error rate is calculated as 1.31% approximately for the step size 1 and 1.11% for 0.1 from the Equation (3.4).

Table 4.6. Newton-Raphson iteration for hexane with $\Delta = 1$ and $\Delta = 0.1$

Iteration	ϵ_r $(\Delta = 1)$	h $(\Delta = 1)$	ϵ_r $(\Delta = 0.1)$	h $(\Delta = 0.1)$
0	1	0.8423	1	0.5827
1	1.8423	0.0355	1.5827	0.2445
2	1.8778	-0.0137	1.8272	0.0312
3	1.864	0.0031	1.8584	0.008
4	1.8671	0.0175	1.8664	0.0152
5	1.8846	-0.0537	1.8816	-0.0626
6	1.831	0.051	1.819	0.0832
7	1.882	-0.0655	1.9022	-0.119
8	1.8165	0.1186	1.7832	0.0663
9	1.9351	-0.0446	1.8495	0.0363
10	1.8905	-0.0802	1.8858	-0.0437
11	1.8103	0.1402	1.8421	0.0256
12	1.9505	-0.0613	1.8677	-0.0018
13	1.8892	-0.0081	1.8659	0.0032
14	1.8811	-0.0478	1.8691	-0.000578
15	1.8333	0.0191		
16	1.8524	0.0158		
17	1.8682	0.0207		
18	1.8889	-0.0028		
19	1.8861	-0.007		
20	1.8791	-0.0138		
21	1.8653	0.000605		

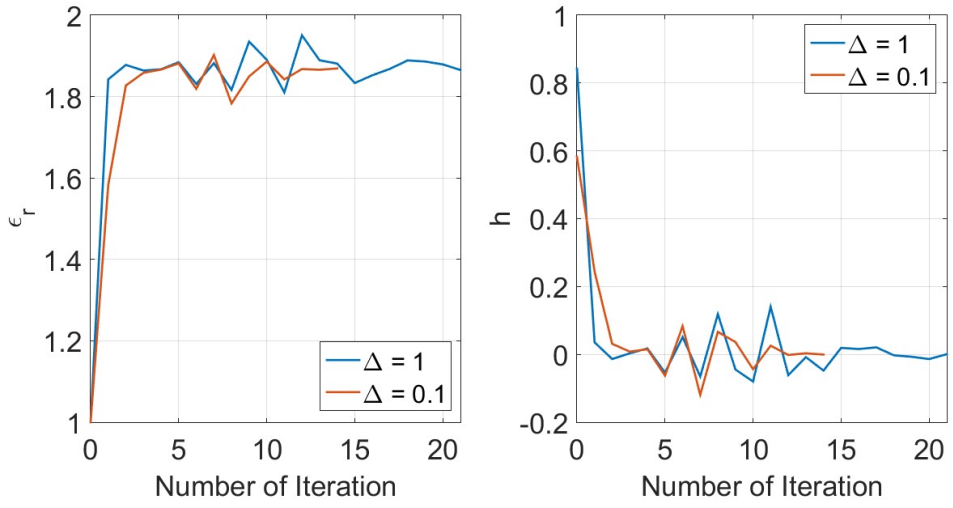

Figure 4.13. Reconstructed dielectric constants and update parameters for hexane

Processing the Newton-Raphson approach, a significant decrease in the error rate is detected. As in the previous simulation test, when the Δ value is high, the desired value is reached faster. Although the number of iterations for the step size 1 is over than of the step size 0.1, the result closer to the desired value is achieved in the first iteration.

Same iterations are repeated for water-added ethanol (see Figure 4.14 and Table 4.7) and drinking water (see Figure 4.16 and Table 4.9) with the same initial point and the same step sizes. In addition, for ethanol samples produced at different water levels, iteration was applied while the step size was 1 as can be examined from Figure 4.15 and Table 4.8. The stopping criterion is determined as 10^{-3}, and if the update parameter become less than 10^{-3} the iteration is completed.

Table 4.7. Newton-Raphson iteration for ethanol 96% with $\Delta = 1$ and $\Delta = 0.1$

Iteration	ϵ_r $(\Delta = 1)$	h $(\Delta = 1)$	ϵ_r $(\Delta = 0.1)$	h $(\Delta = 0.1)$
0	1	14.329	1	6.8515
1	15.329	1.398	7.8515	8.7562
2	16.727	-0.1607	16.6077	0.1559
3	16.5663	0.0206	16.7636	-0.1531
4	16.5869	-0.068	16.6105	-0.0537
5	16.5189	-0.0047	16.5568	0.1174
6	16.5142	-0.0824	16.6742	-0.2608
7	16.4318	0.1278	16.4134	0.2381
8	16.5596	-0.1175	16.6515	-0.2062
9	16.4421	0.0357	16.4453	0.167
10	16.4778	0.0442	16.6123	-0.0665
11	16.522	-0.0332	16.5458	-0.0194
12	16.4888	-0.00091	16.5264	0.0069
13			16.5333	-0.0568
14			16.4765	0.0831
15			16.5596	0.0554
16			16.615	-0.0067
17			16.6083	0.0156
18			16.6239	-0.1155
19			16.5084	0.0663
20			16.5747	-0.0122
21			16.5625	-0.000106

In ethanol 96% measurements, if the step size is 1 the reconstructed value reaches about 16.49, and it is 16.56 while the step size is 0.1. The dielectric constant of ethanol 96% is calculated as 16.64 by considering the amount of water it contains. It can be deduced that the error rate decreases from 17.5% to less than 1% compared to the material

perturbation result. The change of the reconstructed dielectric constant and the update parameter can also be considered from Figure 4.14.

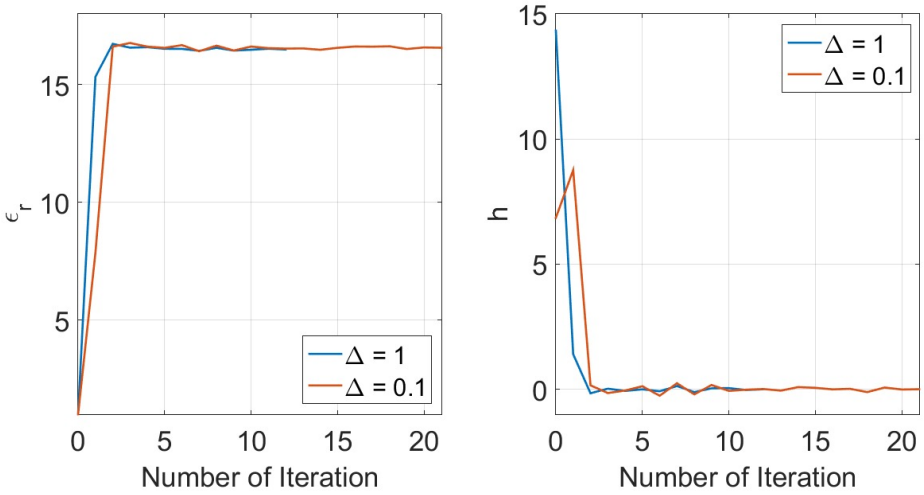

Figure 4.14. Reconstructed dielectric constants and update parameters for ethanol 96%

By adding different levels of distilled water into the ethanol, 2 samples between dielectric constants of ethanol and drinking water were obtained. In addition to the material perturbation method, dielectric constants of these samples were obtained with the Newton-type approach. The results were reached as expected, and although the dielectric constant increased, the Newton-type technique was observed to provide correct results.

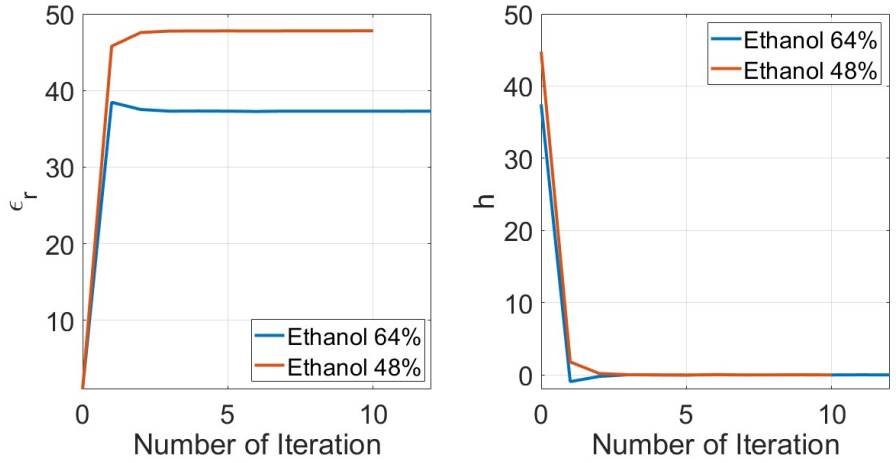

Figure 4.15. Reconstructed dielectric constants and update parameters for ethanol 64% and ethanol 48%

The reconstructed dielectric constants for ethanol 64% and ethanol 48% can be examined from Figure 4.15 and Table 4.8. For ethanol 64%, the calculated real dielectric constant is 37.76 and the reconstructed dielectric constant was obtained as 37.3. The error rate is approximately 1.22%. For ethanol 48%, the reconstructed dielectric constant was obtained as 47.8 and the error rate is calculated as 1.08% according to the exact dielectric constant value 48.32.

Table 4.8. Newton-Raphson iteration for ethanol 64% and 48% with $\Delta = 1$

Iteration	$\epsilon_{r,64\%}$ $(\Delta = 1)$	$h_{64\%}$ $(\Delta = 1)$	$\epsilon_{r,48\%}$ $(\Delta = 1)$	$h_{48\%}$ $(\Delta = 1)$
0	1	37.4574	1	44.7735
1	38.4574	-0.9377	45.7735	1.7912
2	37.5197	-0.2179	47.5647	0.1896
3	37.3018	0.0189	47.7543	0.0151
4	37.3207	-0.0181	47.7694	0.0059
5	37.3026	-0.0399	47.7753	-0.0088
6	37.2627	0.0446	47.7665	0.008
7	37.3073	-0.0097	47.7745	0.0024
8	37.2976	-0.0018	47.7769	0.0041
9	37.2958	0.0069	47.781	0.0165
10	37.3027	-0.0089	47.7975	-0.000703
11	37.2938	0.0078		
12	37.3016	-0.00054		

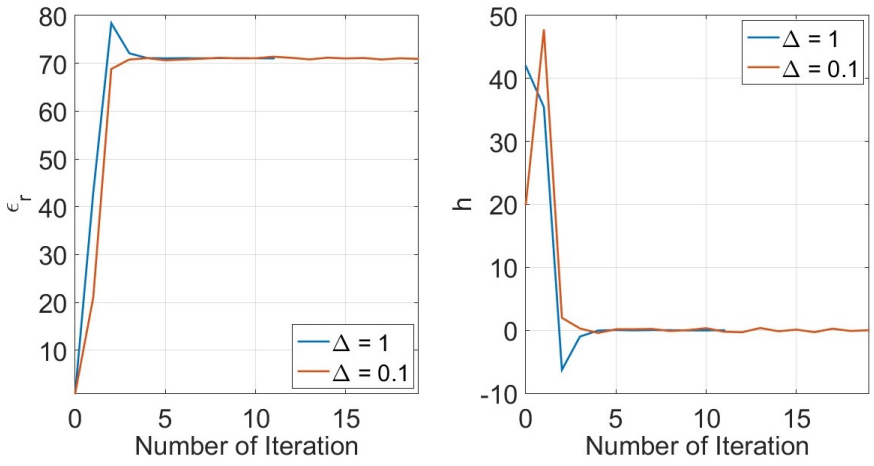

Figure 4.16. Reconstructed dielectric constants and update parameters for water

The Newton method is considered to be beneficial especially in samples with high dielectric constant. The dielectric constant of drinking water in the literature is denoted

as 71.7 at room temperature. In the material perturbation technique, the reconstructed value is detected ∼52 and the error rate is calculated 27.18%. The error rate of ∼1% is observed relating to the dielectric constant approximated to 71 with the Newton-Raphson approach.

Table 4.9. Newton-Raphson iteration for water with $\Delta = 1$ and $\Delta = 0.1$

Iteration	ϵ_r $(\Delta = 1)$	h $(\Delta = 1)$	ϵ_r $(\Delta = 0.1)$	h $(\Delta = 0.1)$
0	1	41.9324	1	20.034
1	42.9324	35.4561	21.034	47.7871
2	78.3885	-6.2933	68.8211	1.9732
3	72.0952	-1.0061	70.7943	0.2829
4	71.0891	-0.0513	71.0772	-0.4331
5	71.0378	0.0339	70.6441	0.1517
6	71.0717	-0.0224	70.7958	0.1603
7	71.0493	0.0282	70.9561	0.2045
8	71.0775	0.0062	71.1606	-0.1275
9	71.0837	-0.0298	71.0331	0.0245
10	71.0539	-0.0267	71.0576	0.3182
11	71.0272	-0.00031	71.3758	-0.2344
12			71.1414	-0.318
13			70.8234	0.3553
14			71.1787	-0.1632
15			71.0155	0.0921
16			71.1076	-0.3044
17			70.8032	0.2422
18			71.0454	-0.1146
19			70.9308	-0.000988

Determination of the dielectric constant of drinking water was examined again by choosing the initial point to 50 (see Figure 4.17 and Table 4.10). In the CST program, a sample with a dielectric constant of 50 was defined and iteration was started with simulation data. Similar results were obtained in iterations with the Newton-type approach in the case of the initial point was air. The dielectric constant of water was found to be 71 approximately, similar to the previous case.

The most dominant error reason for the dielectric constant determination with power measurement is the sensitivity of the spectrum analyzer. Displaying power values in 0.17 unit intervals obstructs to assign some values correctly. In addition, there are conditions that cannot be made exactly the same during measurements, such as fixing the glass tube with silicone and the cover of the cavity.

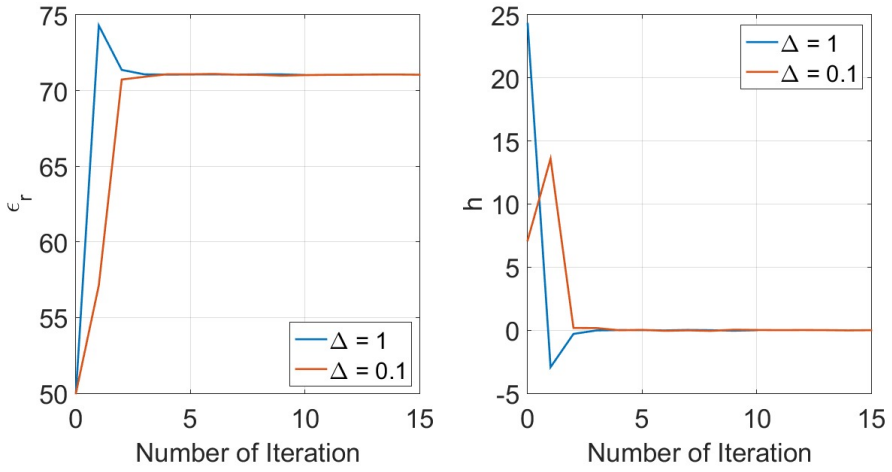

Figure 4.17. Reconstructed dielectric constants and update parameters for water while the initial point $\epsilon_1 = 50$

Table 4.10. Newton-Raphson iteration for water while the initial point $\epsilon_1 = 50$

Iteration	ϵ_r $(\Delta = 1)$	h $(\Delta = 1)$	ϵ_r $(\Delta = 0.1)$	h $(\Delta = 0.1)$
0	50	24.2925	50	7.1308
1	74.2925	-2.9293	57.1308	13.5983
2	71.3632	-0.2945	70.7291	0.1794
3	71.0687	-0.0172	70.9085	0.1686
4	71.0515	0.0092	71.0771	-0.004
5	71.0607	0.0076	71.0731	0.0242
6	71.0683	-0.0172	71.0973	-0.0472
7	71.0511	0.0178	71.0501	-0.0134
8	71.0689	-0.0024	71.0367	-0.0533
9	71.0665	-0.0384	70.9834	0.0382
10	71.0281	-0.000312	71.0216	0.0167
11			71.0383	0.0043
12			71.0426	0.0125
13			71.0551	0.0042
14			71.0593	-0.0144
15			71.0449	-0.00024

CHAPTER 5

CONCLUSION

In this thesis, an iterative approach was proposed to improve sensitivity in dielectric measurements. The applicability of this proposed method was tested with experimental data obtained from microwave cavity measurements. The technique was compared with the conventional method in terms of error rate and the typical convergence behaviours of Newton-type methods was illustrated. The accuracy of the results of the cylindrical and rectangular cavities, which can be utilised with the material perturbation method that is commonly used in dielectric measurements, were evaluated depending on the frequency and dielectric constant. The advantages and disadvantages of the methods were revealed by taking measurements of particular samples both with the conventional technique and with the iterative approach.

Before using the material perturbation method, the results of the cavities were compared. First of all, rectangular and cylindrical cavities with the same volumes at 3 GHz frequency were designed in CST-MWS program. It was observed that as the dielectric constant raised, there was an increment in the error rate for both cavities proportionally, so the perturbation approach is not a convenient technique for the large dielectric constants. The cylindrical cavity yielded more accurate results than the rectangular cavity at high dielectric constant values. When the comparison was considered as the frequency increments throughout the S-band, it was noticed that the rectangular cavity gives more stable results with the increase in frequency. Concluded that in cases where the ratio of cavity volume to the sample volume is low, it is recommended to choose a rectangular cavity for dielectric measurements using perturbation method to obtain more accurate results. Accordingly, dielectric measurements with the material perturbation theory were carried out with 3 different samples as hexane, ethanol and drinking water using a metallic rectangular cavity. Samples of three different water concentration levels were produced for ethanol. The materials were filled in the glass tube and placed in the centre of the cavity. The cavity was excited with a loop antenna and S_{11} parameters were measured with VNA. The necessary reference frequency was chosen from the frequency of the empty cavity. Although the dielectric constant of hexane in the literature is 1.89, it was detected as 1.71. Since there was 4% water in ethanol, the dielectric constant was calculated as 16.64, and 13.73 was achieved by the perturbation method. The calculated exact dielectric constant

values were 37.76 for ethanol 64% and 48.32 for ethanol 64%. The reconstructed dielectric constants were achieved as 30.003 and 37.92 respectively. The dielectric constant of drinking water at room temperature is 71.7, but it was obtained as 52.21. Error rates were calculated as 9.52%, 17.49%, 20.54%, 21.52% and 27.18%, respectively. In this way, the increment in the error rate was verified experimentally as the dielectric constant increased.

An alternative approach was necessary to treat the high error rate in the traditional material perturbation method. For this reason, the Newton-Raphson based dielectric measurement technique was proposed. The effect of three variables as the initial guess, step size and the desired value to be reached was examined with simulations. Simulations were performed for the direct problem whose aim is to obtain the electric field magnitudes of the unknown dielectric parameter. Field values were taken from the curve drawn around the material placed in the middle of the cavity at a particular distance. For finding the unknown dielectric constant which corresponds to the aim of our inverse problem, the Newton-Raphson iterations were used. We started iterations with an initially guessed dielectric constant value and updated at each step. The updated values were found from the solution of an overdetermined system which relates the electric field values to the dielectric constant. Iterations were made for different step size values. While the big step size value provided to reach the final value quickly, the small step size increased the sensitivity. Furthermore, the reconstructions of different dielectric constants by considering various initial guesses were analyzed. Convergence to the desired value was achieved in all simulations carried out with our approach, and the error rate was always below 1%. Iterations were stopped when the update parameter approached to 10^{-3}. In this method, the sensitivity can be increased by reducing the stopping criterion.

Power measurements were carried out with a spectrum analyzer to obtain the electric field strengths inside the cavity. The same cavity and the same samples in the material perturbation method were employed. Firstly, the empty cavity was measured and the system was calibrated with the simulation results received in CST-MWS. The normalization constants obtained by the calibration were utilised to ensure compatibility between power measurements from the spectrum analyzer and simulations. Measurements were individually taken from six ports placed on the cover of the cavity for three different samples. For finding the dielectric constants using the iterative algorithm, the step size was determined two different values as 1 and 0.1, and the stopping criterion was defined as 10^{-3}. The initial guess was considered as 1 which corresponds to the relative dielectric constant of air. Afterwards, we could start iterations by using the measured electric field values for

the first iteration. For the next iterations, we solved the direct problem whose aim is to find electric field values inside the cavity, for the updated dielectric constant with the help of CST simulation which models the measurement setup. For hexane, dielectric constant values approached to 1.87. The final value for ethanol 96% converged to about 16.5. For ethanol 64% and ethanol 48%, the reconstructed dielectric constant values were reached 37.3 and 47.8. The dielectric constant of water was obtained at about 71. While the step size was 1, error rates were 1.31%, 0.91%, 1.22%, 1.08% and 0.98%, respectively. When the step size was 0.1, the error rates were calculated as 1.11%, 0.47% and 1.07%, respectively. When all results were evaluated, the Newton-Raphson approach gave more precise results. For ethanol samples produced with different water concentrations, the reason for the higher error rate is volumetric errors. The spectrum analyzer used had a sensitivity of 0.17 dB. More accurate results could be achieved with more sensitive measuring devices.

Although the proposed procedure gives more accurate results, it needs a solution to the directive problem at each iteration step. Depending on the computational sources the solution of the direct problem with a full Maxwell solver might be time-consuming. Furthermore, the direct problems should be computed sufficiently accurate otherwise the results might not converge to the searched exact dielectric constant value. On the other hand, our approach cancels out fundamental limitations of classical perturbation method, i.e. with the iterative method it is possible to find large dielectric constant, one does not need to excite a certain mode inside the cavity. The proposed approach has more precise results and the error rate for high dielectric constants is quite low. In addition, while the sample volumes should be small in the perturbation technique, there is no dependence on the material volume in this method. The dielectric constant is a frequency-dependent variable. When measuring a sample whose dielectric constant is unexplored by using the material perturbation approach, how much shifting frequency will occur cannot be predicted. However, in the proposed process, all measurements are taken at a certain frequency. Thus, frequency dependence was also eliminated. The cavity does not need to be excited by any mode therefore the coupling conditions of the excitation are more relaxed. This is the only point to be considered in frequency selection.

The advantages of the proposed technique consequently dominate its disadvantages in a major way. In this thesis, the iterative Newton-Raphson based approach is compared with traditional methods, and its applicability with simulations and measurements is presented.

REFERENCES

Abdelgwad, Aahmad and Tarek Said (2015). Measured dielectric permittivity of chlorinated drinking water in the microwave frequency range. In *2015 IEEE 15th Mediterranean Microwave Symposium (MMS)*, pp. 1–4.

Baker-Jarvis, James, Michael D. Janezic, and Donald C. Degroot (2010, April). High-frequency dielectric measurements. *IEEE Instrumentation & Measurement Magazine 13*(2), 24–31.

Balanis, Constantine A. (2012). *Advanced Engineering Electromagnetics, 2nd Edition*. Wiley.

Bickel, Peter J. and Kjell A. Doksum (2007). *Mathematical Statistics: Basic Ideas and Selected Topics*. Pearson Prentice Hall.

Carter, Richard G. (2001a). Accuracy of microwave cavity perturbation measurements. *IEEE Transactions on Microwave Theory and Techniques 49*(5), 918–923.

Carter, Richard G. (2001b). Accuracy of microwave cavity perturbation measurements. *IEEE Transactions on Microwave Theory and Techniques 49*(5), 918–923.

Chen, Linfeng, CK Ong, CP Neo, Vasundara Varadan, and Vijay K. Varadan (2004). *Microwave Electronics: Measurement and Materials Characterization*. Wiley.

Clerjon, Sylvie and Jean-Louis Damez (2009). Microwave sensing for an objective evaluation of meat ageing. *Journal of Food Engineering 94*(3), 379 – 389.

CST MICROWAVE STUDIO (2018). CST AG - Computer Simulation Technology, Darmstadt, Germany. [online] Available: http://www.cst.com.

Debye, Peter (1929). *Polar Molecules*. New York: NY: The Chemical Catalog Company.

Dunlap, Crawford and Benjamin Makower (1945). Radio-frequency dielectric properties of dehydrated carrots. application to moisture determination by electrical methods. *The Journal of Physical Chemistry 49*(6), 601–622.

Ghodgaonkar, Deepak, Vasundara Varadan, and Vijay K. Varadan (1990, April). Free-space measurement of complex permittivity and complex permeability of magnetic materials at microwave frequencies. *IEEE Transactions on Instrumentation and Measurement 39*(2), 387–394.

Hakki, Basil, and Paul D. Coleman (1960, July). A dielectric resonator method of measuring inductive capacities in the millimeter range. *IRE Transactions on Microwave Theory and Techniques 8*(4), 402–410.

Hayakawa, Toshiro and Koichiro Sawa (1997). Breaking arc in several liquid environments with light-duty application. In *Electrical Contacts - 1997 Proceedings of the Forty-Third IEEE Holm Conference on Electrical Contacts*, pp. 246–253.

Hu, Jiqing, Arien Sligar, Chih-Hung Chang, Shih-Lien Lu, and Raghu K. Settaluri (2006, July). A grounded coplanar waveguide technique for microwave measurement of complex permittivity and permeability. *IEEE Transactions on Magnetics 42*(7), 1929–1931.

Jha, Abhishek Kumar and Mohammad Jaleel Akhtar (2014, Nov). A generalized rectangular cavity approach for determination of complex permittivity of materials. *IEEE Transactions on Instrumentation and Measurement 63*(11), 2632–2641.

Jilani, Muhammad Taha (2012, 12). A brief review of measuring techniques for characterization of dielectric materials. *International Journal of Information Technology and Electrical Engineering*.

Kaczkowski, Andrzej and Andrzej Milewski (1980, Mar). High-accuracy wide-range measurement method for determination of complex permittivity in reentrant cavity: Part a - theoretical analysis of the method. *IEEE Transactions on Microwave Theory and Techniques 28*(3), 225–228.

Kik, Alfred (2016). Complex permittivity measurement using a ridged waveguide cavity and the perturbation method. *IEEE Transactions on Microwave Theory and Techniques 64*(11), 3878–3886.

Kilic, Emre, Uwe Siart, Oliver Wiedenmann, Usman Faz, Robert Ramakrishnan, Patrick

Saal, and Thomas F. Eibert (2013). Cavity resonator measurement of dielectric materials accounting for wall losses and a filling hole. *IEEE Transactions on Instrumentation and Measurement 62*(2), 401–407.

Krupka, Jerzy (2006). Frequency domain complex permittivity measurements at microwave frequencies. *Meas. Sci. Technol. 17*, 55 – 70.

Li, Shihe, Cevdet Akyel, Renato G. Bosisio (1981, Oct). Precise calculations and measurements on the complex dielectric constant of lossy materials using tm/sub 010/ cavity perturbation techniques. *IEEE Transactions on Microwave Theory and Techniques 29*(10), 1041–1048.

Nelson, Stuart (1965, 01). Dielectric properties of grain and seed in the 1 to 50-mc range. *Transactions of the ASAE 8*, 0038–0048.

Nelson, Stuart O. and Philip G. Bartley (2002, Aug). Measuring frequency- and temperature-dependent permittivities of food materials. *IEEE Transactions on Instrumentation and Measurement 51*(4), 589–592.

Nishikata, Atsuhiro (2009). Scattering analysis for layered cylindrical object perpendicularly piercing the wider walls of a rectangular waveguide and its application to ε_r and μ_r measurement. *IEEE Transactions on Microwave Theory and Techniques 57*(6), 1602–1611.

Ogunlade, Olumide, Roger D. Pollard and Ian C. Hunter (2006, June). A new method of obtaining the permittivity of liquids using in-waveguide technique. *IEEE Microwave and Wireless Components Letters 16*(6), 363–365.

Ostrowski, Alexander (1966). *Solution of Equations and Systems of Equations*. New York and London: Academic Press.

Ozkal, Ceren and Fatih Yaman (2018, 9). The cavity perturbation method for the dielectric constants measurements. In *Turkish Physical Society 34th International Physics Congress*, Bodrum, Turkey.

Ozkal, Ceren and Fatih Yaman (2019). Investigations for increasing the accuracy of dielectric constant measurements. In *Book of Full Text Proceedings Turkish Physical*

Society 35th International Physics Congress (TPS35), Volume 01, Bodrum, Turkey, pp. 74–81.

Peng, Zhiwei, Jiann-Yang Hwang and Matthew Andriese (2014). Maximum sample volume for permittivity measurements by cavity perturbation technique. *IEEE Transactions on Instrumentation and Measurement 63*(2), 450–455.

Pozar, David M. (2012). *Microwave Engineering*. Hoboken, NJ: Wiley.

Puvvadi, Satheshbabu, C.V.S Subrahmanyam, Thimmasetty Juturu, R. Manavalan, Kannappan Valliappan, and Senepati Kedarnath (2008, 01). Solubility enhancement of cox-ii inhibitors by cosolvency approach. *Dhaka University Journal of Pharmaceutical Sciences 7*.

R. Zajicek, J. Vrba, K. N. (2006). Evaluation of a reflection method on an open-ended coaxial line and its use in dielectric measurements. *Acta Polytechnica 46*(5), 50–54.

Riedell, Heyward, Michael B. Steer, and Mike R. Kay, Jefferey S. Kasten, Mark S. Basel, and Real Pomerleau (1990, April). Dielectric characterization of printed circuit board substrates. *IEEE Transactions on Instrumentation and Measurement 39*(2), 437–440.

Sadiku, Matthew (2000). *Numerical Techniques in Electromagnetics with Matlab*. CRC Press.

Santra, Mrityunjay and K.U. Limaye (2005). Estimation of complex permittivity of arbitrary shape and size dielectric samples using cavity measurement technique at microwave frequencies. *IEEE Transactions on Microwave Theory and Techniques 53*(2), 718–722.

Sato, Takaaki and Richard Buchner (2004). Dielectric relaxation processes in ethanol/water mixtures. *The Journal of Physical Chemistry A 108*(23), 5007–5015.

Sheen, Jyh (2007, October). Microwave measurements of dielectric properties using a closed cylindrical cavity dielectric resonator. *IEEE Transactions on Dielectrics and Electrical Insulation 14*(5), 1139–1144.

Shu, Y. and T. Y. Wong (1995, April). Perturbation of dielectric resonator for material measurement. *Electronics Letters 31*(9), 704–705.

Teng, Alex, Muhammad Ateeq, Andrew Shaw A. Al-Shamma, S.N. Kazi and B.T. Chew and Patryk Kot (2017, 02). Numerical investigation on using an electromagnetic wave sensor to detect water hardness in water cooling system industry. *International Journal of Electromagnetics and Applications 7*(2), 38–47.

von Hippel, Arthur (1954a). *Dielectric Materials and Applications*. New York: Wiley/The Technology Press of MIT.

von Hippel, Arthur (1954b). *Dielectrics and Waves*. New York: NY: John Wiley and Sons.

Wee, Fwen Hoon and Ping Jack Soh and A. H. M. Suhaizal and H. Nornikman, and Muhammad Ezanuddin Abdul Aziz (2009, Nov). Free space measurement technique on dielectric properties of agricultural residues at microwave frequencies. In *2009 SBMO/IEEE MTT-S International Microwave and Optoelectronics Conference (IMOC)*, pp. 183–187.